



**Titre:** Automatic incorporation of circular riverbank failures in two-dimensional flood modeling

**Auteurs:** Ismail Ouchebri, & Tew-Fik Mahdi

**Date:** 2021

**Type:** Article de revue / Article


**Référence:** Ouchebri, I., & Mahdi, T.-F. (2021). Automatic incorporation of circular riverbank failures in two-dimensional flood modeling. Canadian Journal of Civil Engineering, 48(8), 1004-1019. <https://doi.org/10.1139/cjce-2019-0670>

 **Document en libre accès dans PolyPublie**  
Open Access document in PolyPublie

**URL de PolyPublie:** <https://publications.polymtl.ca/5478/>

**Version:** Version finale avant publication / Accepted version  
Révisé par les pairs / Refereed

**Conditions d'utilisation:** Tous droits réservés / All rights reserved

 **Document publié chez l'éditeur officiel**  
Document issued by the official publisher

**Titre de la revue:** Canadian Journal of Civil Engineering (vol. 48, no. 8)

**Maison d'édition:** Canadian Science Publishing

**URL officiel:** <https://doi.org/10.1139/cjce-2019-0670>

**Mention légale:** ©2021. This is the author's version of an article that appeared in Canadian Journal of Civil Engineering (vol. 48, no. 8) . The final published version is available at <https://doi.org/10.1139/cjce-2019-0670>

# 1 **AUTOMATIC INCORPORATION OF RIVERBANK FAILURES IN TWO-** 2 **DIMENSIONAL FLOOD MODELING**

3 Ouchebri, Ismail<sup>1</sup>; Mahdi, Tew-Fik<sup>2</sup>

4 <sup>1</sup> Ph.D Student, Département des génies Civil, Géologique et des Mines (CGM), École Polytechnique de  
5 Montréal, C.P. 6079, succursale Centre-Ville, Montréal, QC H3C 3A7, Canada. Email:  
6 ismail.ouchebri@polymtl.ca

7 <sup>2</sup> Professor, Département des génies Civil, Géologique et des Mines (CGM), École Polytechnique de  
8 Montréal, C.P. 6079, succursale Centre-Ville, Montréal, QC H3C 3A7, Canada (Corresponding author).  
9 Email: tewfik.mahdi@polymtl.ca

## 10 **Abstract**

11 Riverbanks undergo changes caused not only by river hydraulics, mainly sediment erosion and deposition  
12 processes, but also by the possible landslides that eventually change the channel bank profiles. Those  
13 failures are an important form of alluvial channel adjustments but are usually difficult to include during  
14 morphodynamic modeling. This paper proposes a novel approach combining a 2D depth-averaged  
15 hydrodynamic, sediment transport and mobile-bed model, SRH-2D, a limit equilibrium slope-stability  
16 model, BISHOP, and a bank failure sediment redistribution submodel, REDISSED, into a fully automatic  
17 and continuous dynamic simulation to predict vertical bed and lateral bank changes for a river reach  
18 undergoing exceptional flooding. The in-stream vertical fluvial changes predicted with the SRH-2D model  
19 will be automatically used to update the riverbank geometry profile by profile and assess their  
20 geotechnical stability to rotational slip failures with a developed slope-stability model based on Bishop's  
21 simplified method. A cone-shaped sliding area is defined in case the driving forces exceed the stabilizing  
22 forces. All mesh nodes located within the mass wasting zone will be automatically updated, allowing a  
23 new bank face form. The failed materials will be redistributed in the transect according to the geometry of  
24 the landslides observed at the study site. The Outaouais River at Notre-Dame-Du Nord, Quebec, is used  
25 to test the coupling procedure. Up to 100 m of bank retreat was predicted, and more than 20 cross-

26 sections were reshaped. Typical results showing the effectiveness of the developed framework are  
27 presented and discussed.

28 **Author keywords:** Streambank erosion; Riverbank failure; Two-dimensional modeling; SRH-2D;  
29 BISHOP; Automatic coupling; Sediment redistribution.

## 30 **Introduction**

31 Rivers are dynamic systems governed by hydraulic and sediment transport processes. Over time,  
32 meandering channels respond to changing conditions in the environment by modifying their cross-  
33 sectional and planform shapes. In fact, alluvial rivers in nature display morphological adjustments in  
34 response to the exerted stresses, especially erosion, triggered by the interaction of flow and the riverbed  
35 or banks. Streambank erosion is considered one of the most important processes in adjusting alluvial  
36 systems (Langendoen et al. 2009). It is a natural process that occurs when the forces exerted by flowing  
37 water exceed the resisting forces of the bank materials and vegetation (Simon et al. 2000). This type of  
38 erosion is generally regarded as a combination of the fluvial entrainment of bank materials by flowing  
39 water and the mass failure of unstable banks (ASCE Task Committee on Hydraulics 1998; Darby et al.  
40 2007; Langendoen and Simon 2008). From a numerical perspective, riverbank failures are often  
41 overlooked when modeling channel morphological evolution; the multidimensional hydrodynamic and bed  
42 evolution models only evaluate fluvial erosion and need to be coupled with bank erosion submodels to  
43 assess channel morphological adjustments evoked by riverbank geotechnical mass failures.

44 To properly examine river morphological evolution, researchers and practitioners have established a large  
45 number of assumptions, developed tools and models and utilized different approaches and techniques to  
46 combine both fluvial erosion and mass wasting (Lai et al. 2012; Lai et al. 2015; Langendoen et al. 2016;  
47 Langendoen and Simon 2008; Mahdi and Marche 2003; Rousseau et al. 2017). Notwithstanding the  
48 various employed strategies, they all aim to integrate the different physical processes responsible for  
49 bank retreat into one runnable solution by coupling physical and process-based models. One of those  
50 solutions consisted of combining the flowing-water and bank erosion computer models with mass failure  
51 predictive models. (Mahdi and Marche 2003) were probably the first to simulate the morphologic  
52 adjustment of both the bed and the banks over a long river reach (9.8 km) in a natural meandering river

53 system by coupling one-dimensional (1D) erosion and sediment transport model GSTARS-1D (Yang et al.  
54 1998) with a bank-stability model called BISHOP to assess the circular failures of nonhomogenous  
55 cohesive banks (Mahdi and Merabtene 2010; Mahdi and Marche 2003); the combined model was later  
56 used to evaluate bank retreat of the river downstream of the Première Chute Dam (Mahdi 2004) in  
57 Quebec and yielded a promising results. However, the mobile-bed model GSTARS-1D (Yang et al. 1998)  
58 uses a simple theory in that the channel geometry adjustments can be vertical or lateral depending on the  
59 minimum unit stream power theory (Yang 1976), an approach that can be used only for short- and  
60 medium-term predictions (Simon et al. 2007). Similarly, (Langendoen and Simon 2008) merged an  
61 unsteady one-dimensional channel evolution and physically based model called CONCEPTS  
62 (Langendoen 2000) with a geotechnical submodel to simulate the streambank planar failures of  
63 riverbanks over the bendway of Goodwin Creek, Mississippi, and later over two incised streams in  
64 northern Mississippi, James Creek and the Yalobusha River (Langendoen et al. 2009). (Motta et al. 2012)  
65 coupled the physically based algorithms of the channel evolution model CONCEPTS (Langendoen 2000)  
66 with the (2D) hydrodynamic and migration RVR Meander model (Abad and Garcia 2006) to simulate  
67 meander migration at the reach scale. Recently, (Motta et al. 2012) simulated bank retreat also using the  
68 one-dimensional computer model CONCEPTS (Langendoen 2000) to investigate the impact of the  
69 variability of erodibility parameters on the model's lateral retreat predictions. However, CONCEPTS  
70 (Langendoen 2000) and likely GSTARS-1D (Yang et al. 1998) are 1D models they do not incorporate  
71 corrections for secondary currents and transversal bed slope, and hydraulics are not adequately resolved  
72 to predict bank erosion. Therefore, their applicability to meander bends might underestimate the shear  
73 stress along the streambank. Indeed, the increased shear stresses for the CONCEPTS (Langendoen  
74 2000) model are represented by a reduction in resistance to erosion of the bank material (Langendoen  
75 and Simon 2008); the model is unable to predict the increased hydraulic forces acting on the outer banks  
76 caused by the helical flow patterns in the bends, which limits its applicability to only in regions where the  
77 phenomena can be neglected (Lai et al. 2012). Moreover, (Abad and Garcia 2006) showed less variation  
78 in predicted retreat by the one-dimensional model compared to the incorporated erodibility parameters  
79 derived from streambank tests and, more importantly, stressed the need for two- or three-dimensional  
80 modeling.

81 The coupling between riverbank mass failure algorithms and one-dimensional computer models was  
82 probably the only way to account for streambank erosion as an important process of river morphological  
83 adjustment, despite the simplified physically based equations implemented and the relevant assumptions  
84 involved. In recent years, researchers have taken advantage of two-dimensional (2D) morphodynamic  
85 numerical models to better understand the interactions between fluvial erosion and mass wasting.  
86 (Rinaldi et al. 2008) enhanced our comprehension of this matter by coupling the different components of  
87 bank retreat separately using the 2D depth-averaged hydrodynamic model (Deltares Delft 3D) with the  
88 commercial groundwater model (GeoSlope, SEEP/W) and the bank stability analysis model (GeoSlope,  
89 SLOPE/W) and applied it in a reach-scale hydraulics study within the river bend of the Cecina River, Italy.  
90 Despite the overall success of highlighting the roles of fluvial erosion and mass failure driven by  
91 hydrodynamic conditions and geotechnical factors, the (Rinaldi et al. 2008) approach loosely accounted  
92 for feedbacks between the eroded bank and the flow and simply ignored bed-level changes. In addition,  
93 the approach is computationally expensive in terms of the time needed for manual remeshing, making it  
94 strictly convenient to simulate a single flood event. Recently, (Rousseau et al. 2017) developed and  
95 coupled a riparian vegetation module and a geotechnical algorithm with the two-dimensional solver  
96 Telemac-Mascaret (Galland et al. 1991) to predict bank retreat for a semialluvial meandering reach  
97 (Medway Creek, Ontario, Canada). The study addressed the effects of plants on the mechanical  
98 properties of riverbanks and evaluated the geotechnical stability of the banks independently of the  
99 hydrodynamic mesh. It is among the rarest studies to include mass wasting and vegetation processes  
100 over a long spatiotemporal scale. (Lai et al. 2015) coupled the deterministic bank stability and toe erosion  
101 model (BSTEM) (Simon et al. 2011) developed by the National Sedimentation Laboratory to the 2D  
102 depth-averaged hydraulic and sediment transport model SHR-2D (Lai 2010) to predict streambank retreat  
103 and planform development. (Lai et al. 2015) evaluated the bank erosion using the near-bank bed shear  
104 stress computed by SRH-2D (Lai 2010) and manually moved the mesh to account for the bank toe  
105 displacement, an approach that might be very costly in terms of time needed to readjust the mesh and  
106 especially, as the researchers acknowledged, the time required to update and interpolate variables. Later,  
107 (Lai 2017) extended the previous moving mesh approach to the fixed mesh method and showed that it is  
108 often useful to combine both approaches to improve the robustness of the numerical model and thus

109 accurately predict vertical stream bed changes and lateral streambank erosion for complex systems. In  
110 both cases, bank geometries and their erosion are treated separately from SRH-2D (Lai 2010)  
111 components. A strategy that allows adequate representation of the bank geometry is often difficult using  
112 two-dimensional models that generally reduce bank profiles to a single linear segment.

113 The state-of-the-art described above presents the most recent studies coupling multiple versions of one-  
114 dimensional or two-dimensional models simulating both bed and bank adjustments. Most of those studies  
115 are time consuming if applied on a long-reach scale. Moreover, to correctly represent bank geometry  
116 within two-dimensional mobile-bed models, geotechnical evaluations are performed independently from  
117 the mesh. Thus, in the case of bank retreat, the mesh needs to be readjusted manually, which makes the  
118 coupling procedure strictly practical on a limited-size channel. Furthermore, since there is no consensus  
119 among researchers considering the redistribution of the derived bank materials, morphodynamical studies  
120 simply omit or utilize *ad hoc* approaches to redeposit the failed blocks (Darby and Delbono 2002; Nagata  
121 et al. 2000; Pizzuto 1990). In this article, the authors aim to overcome these difficulties by developing a  
122 new platform capable of the following: first, describing adequately the stratigraphy and bank geometry of  
123 the cross-sections, along which slope-stability assessments are performed, in a 2D mesh without  
124 necessarily needing to idealize them; second, assessing their geotechnical stability to rotational failures  
125 using an automatic search routine capable of identifying the minimum factor of safety at the potentially  
126 unstable riverbanks; third, and most importantly, redistributing slump blocks onto the 2D mesh based on  
127 the topographic form of the failed materials in the study area while conserving the mass; and fourth,  
128 simulating the feedbacks between the coupled models at each time step automatically, including the  
129 mesh movement, without user intervention. The developed procedure is an easy-to-use and time-saving  
130 tool for evaluating streambank retreat due to both fluvial erosion and geotechnical failure in long-reach  
131 scale modeling systems. Details of the pairing scheme are described in the following sections. The model  
132 is applied to the analysis of the evolution of a river reach several kilometers downstream of a dam break  
133 scenario.

## 134 **Overview of the model components**

135 In the present modeling investigation, we combine the 2D mobile-bed model SRH-2D (Lai 2008; Lai  
136 2010) with the slope stability model BISHOP (Mahdi 2004; Mahdi and Merabtene 2010) and the riverbank  
137 failed materials redistribution submodel REDISSED (Mahdi 2004). In the following, the models are  
138 presented first, and their coupling is then described and discussed.

### 139 **SRH-2D Model**

140 The SRH-2D (Sedimentation and River Hydraulics - Two-Dimensional) model (Lai 2008; Lai 2010) is a  
141 two-dimensional flow, mobile-bed and sediment transport model developed by the U.S. Bureau of  
142 Reclamation. The model is flexible; it uses an unstructured hybrid mesh numerical method that can be  
143 applied to arbitrarily shaped cells. Moreover, SRH-2D solves the 2D dynamic wave equations, i.e., the  
144 depth-averaged St. Venant equations, with a very robust and stable numerical scheme based on a finite  
145 volume discretization. In terms of hydrodynamic modeling capabilities, SRH-2D has shown its capacities  
146 for hydraulic calculations compared to Hydro\_As-2D (Lavoie and Mahdi 2017) and was previously tested  
147 successfully in many other studies (Lai et al. 2010; Lai et al. 2016; Moges 2010).

148 For a complete analysis within SRH-2D, the model needs a mesh generator. Since the model adopts the  
149 arbitrarily shaped mesh system, any 2D mesh generator program may be used. At present, SRH-2D uses  
150 the SMS model (AQUAVEO 2019) as the mesh generator and postprocessing graphical model. A typical  
151 modeling consists of delimiting the initial solution domain on the SMS, defining the topographic and  
152 bathymetric data, assigning the channel's materials and boundary conditions and finally generating the  
153 mesh. Within the SMS, it is possible to run SRH-2D for single simulation or to export all the simulation  
154 data into files for future use, an approach that will be adopted in this study. The authors will use the  
155 exported data to launch the SRH-2D processor (*srh-2d*). The model outputs the results files that describe  
156 the time-dependent evolution of the cross-sections. Several forms of data processing can be considered.

### 157 **BISHOP Model**

158 BISHOP is a geotechnical stability analysis model developed by (Mahdi 2004) to evaluate bank profile  
159 stability. The model iteratively calculates the minimum factor of safety based on Bishop's modified method

160 (Philipponnat and Hubert 1979); it isolates the global minimum factor of safety from all the local minima for  
 161 a given slope. Stability analysis is carried out based on the approach of circular failures, a type of  
 162 riverbank failure often noticed *in situ* (Highland and Bobrowsky 2008; Philipponnat and Hubert 1979) and  
 163 associated with cohesive soils (Thorne 1982). BISHOP has been tested and compared previously to  
 164 other commercial rotational failure software (GeoSlope SLOPE/W) (Fredlund 1995) and has proven its  
 165 ability to accurately evaluate the force equilibrium factor of safety for rotational failures (Mahdi 2004;  
 166 Mahdi and Merabtene 2010). The geotechnical model iteratively calculates the minimum factor of safety  
 167 based on Bishop's modified method (Philipponnat and Hubert 1979) by solving the following implicit  
 168 equation:

$$FS = \frac{\sum_i^N \left( \frac{(W_i - u_i b_i) \tan \phi'_i + c'_i b_i}{\cos \alpha_i + \sin \alpha_i \frac{\tan \phi'_i}{FS}} \right)}{\sum_i^N (W_i \sin \alpha_i)} \quad (1)$$

170

171 In the above,  $FS$  is the factor of safety, and banks are considered unstable when  $FS < 1$ , and for any slice  
 172  $i$  (Fig. 1),  $W_i$  is the weight;  $b_i$  is the river width;  $u_i$  is the pore water pressure at the bottom of the slice;  $\alpha_i$   
 173 is the angle between the vertical and the radius  $R$  of the circular slip surface;  $c'_i$  is the effective cohesion  
 174 and  $\phi'_i$  is the effective angle of friction. In Fig.1,  $H$  refers to the horizontal interslice force, and  $I$  represents  
 175 the center of a trial circle of radius  $R$ . Interested readers can refer to (Mahdi 2004; Mahdi and Merabtene  
 176 2010) for further details concerning the numerical implementation.

177 BISHOP combines the bank geometry and bank soil geotechnical properties (effective cohesion,  
 178 undrained cohesion, interior effective friction angle, and saturated unit weight) in the same input file. One  
 179 to nineteen stratigraphic layers might be defined for each riverbank, with each layer having its own  
 180 geotechnical properties as well as pore water pressure conditions. In addition, the model can be adjusted  
 181 when applied to a watercourse submerged by water; it takes into account the hydrostatic water pressure  
 182 by assuming the surface water as a soil layer of unit weight equal to that of water but with no shear  
 183 strength.



184 The BISHOP model was mainly used in the study instead of conventional software (i.e., GeoSlope,  
185 SLOPE/W) to facilitate the automatic coupling of the models. In fact, the conventional software were  
186 avoided since they require the model user to draw the bank profile and its different geotechnical layers as  
187 well as the groundwater table, which is impractical in this study since many hydraulic cross-sections must  
188 be analyzed during the flooding event which will be tedious and time consuming to do for each riverbank.

### 189 **REDISSED Submodel**

190 REDISSED is a sediment redistribution submodel developed by (Mahdi 2004) to reshape the bank  
191 profiles following a circular failure. The model conserves the mass and accommodates the observed  
192 failure form of the banks in the study site. In the case of bank failure, the model redistributes the bank-  
193 derived materials in the flow section where their erosion and/or transport will be determined by the  
194 subsequent hydraulic conditions incorporated in the mobile-bed model.

195 As stated above, since there is no consensus among researchers regarding the redistribution of the  
196 derived bank materials (Darby and Delbono 2002; Nagata et al. 2000; Pizzuto 1990), the authors  
197 considered a field-based approach implemented in the REDISSED submodel. It consists of redistributing  
198 the failed materials as follows: The initial bank geometry is first described by a set of points (mesh nodes);  
199 for simplification purposes, we consider the points ABCXZ plotted in Fig. . In the case of bank failure, the  
200 circular sliding surface is along points ADC. The ABCD block is rotated so that the difference in altitude  
201 between A and its image A' will be equal to  $H/\alpha$ , where  $H$  is the failure height (the difference in altitude  
202 between points A and C) and  $\alpha$  is a coefficient greater than unity and is specified by the user based on  
203 observations of the study site. Point B', the image of B, is projected orthogonally to obtain point B'' as  
204 shown in Fig. .

205 Fig. illustrates the new bank profile defined by the points AA'B''C'EZ, where point E belongs to section  
206 XZ, so that A'B'C'B''A' and CC'EXC have equal areas for mass (or area) conservation purposes.

207 In a nutshell, the slump blocks undergo a rotation followed by a translation that moves the upper end of  
208 the sliding bank to the bottom of the cross-section while conserving the mass. Once the submodel  
209 redefines the form of the failed blocks, the topography of the bank section is automatically updated  
210 accordingly before moving on to the next hydraulic time step. Meanwhile, the geotechnical layers are

211 updated through linear interpolation assumptions between the different points defining the geotechnical  
212 layers.

### 213 **Sliding cone area**

214 Redistribution of the mass wasting deposits of the unstable talus will be performed by using REDISSED  
215 (Mahdi 2004) along the predefined cross-sections. However, the unstable failure block is a 2D planar  
216 surface. Hence, to ensure the fully two-dimensional aspect of the study, the authors considered a sliding  
217 bank area in the shape of a right cone with its axis as the cross-section line, its vertex as the upper point  
218 of intersection between the riverbank and the slip circle computed by BISHOP (Mahdi 2004), and its  
219 opening angle is a user-defined parameter (Fig. ). The mesh nodes located within the sliding cone area  
220 will have their topography automatically interpolated to accommodate the new reshaped bank profile. The  
221 mesh nodes affected by the failure will have a vertical displacement according to their position with  
222 respect to the new bank geometry, i.e.,

$$223 \quad Z_M = Z_{B''} + \frac{d_M}{d} \times (Z_{C'} - Z_{B''}) \quad (2)$$

224 where  $Z_M$  is the mesh node elevation obtained by interpolation;  $Z_{B''}$  and  $Z_{C'}$  are the elevations of the  
225 mesh nodes  $B''$  and  $C'$ , respectively, belonging to the new bank profile;  $d_M$  is the distance from the node  
226  $B''$ , the nearest mesh node from node  $M$ ; and  $d$  is the distance between the two mesh nodes  $B''$  and  $C'$ .

227 The choice of the mesh nodes to be used for interpolation is done automatically, and the x coordinate of  
228 the interpolated mesh node ( $M$ ) should be between the abscissa of the two mesh nodes, here nodes  $B''$   
229 and  $C'$ .

### 230 **Coupling SRH-2D and BISHOP-REDISSED**

231 The coupling between models started by incorporating bathymetric and topographic data on the SMS in  
232 a similar fashion to the conventional mobile-bed and sediment transport modeling with SRH-2D, and  
233 defining the cross-sections where the stability analysis will be performed. They will be set as node strings  
234 on the SMS just before generating the mesh (Fig. ). Aftergenerating the mesh (Fig. ) and assigning the

235 boundary conditions, the pre-established cross-sections will be defined as monitor lines (maximum of 98  
236 monitor lines) to get access to their nodes when exporting data. All other necessary modeling inputs  
237 (Manning's roughness, materials, simulation time, and initial conditions) can be fixed; thereafter, the key  
238 simulation data can be exported to three principal files, the most important of which holds the node  
239 coordinates at the monitor lines. This file will be used to ensure automatic feedback between the vertical  
240 changes predicted by the 2D mobile-bed model and the lateral changes predicted by the geotechnical-  
241 stability and sediment-redistribution model BISHOP-REDISSED.

242 Assessing the geotechnical stability of the riverbanks and updating automatically the flow-wise 2D  
243 geometry in case of bank failure for a long-reach-scale system without having to manually move the mesh  
244 is seen as a key contribution of this study. Significant effort was expended to find a suitable procedure to  
245 model hydraulic cross-sections while considering their geotechnical characteristics. Herein, each cross-  
246 section was modeled as a set of vertical lines whose abscissa are the mesh nodes defining the transects.  
247 These vertical lines form points of intersection at each change in the geotechnical properties of the  
248 predefined layers (Fig. ). Thus, two text files are used in compiling geometric and geotechnical data. The  
249 geometric file stores data in a vector whose components are the x-coordinate of the vertical line, the  
250 elevation of the highest point of the cross-section and the elevation of the base of the different  
251 geotechnical layers. We note that it is also possible to include the elevation of the crevice if it exists and  
252 the elevation of the water level in it. Similarly, the geotechnical file regroups the geotechnical properties of  
253 each soil layer for each riverbank profile separately, which includes the values of the effective cohesion  
254  $c'$ , the undrained cohesion  $c_u$ , the unit weight  $\gamma'$  and the interior effective friction angle  $\phi'$  as well as the  
255 elevation of the groundwater table or the pore pressure ratio  $r_u$ . It is worth mentioning that the global  
256 coordinates of the nodes of the mesh in the SMS will be automatically transformed, translated and  
257 rotated to have local coordinates with an origin at the far-left bank node of each cross-section (Node 1 in  
258 Fig. ). These coordinates will be used to define the geometric files for BISHOP model. This is a  
259 fundamental and necessary step since it will avoid distortion when updating the mesh and yet allows  
260 consideration of river sinuosity.

261 Having defined the hydraulic and geotechnical parameters, the next step consists of launching the  
262 developed automation algorithm. With a text-based interactive user interface, the user defines the case  
263 name, the number of cross-sections, the slope of the potential sliding cone and finally the time step  $\Delta t'$  to  
264 test the stability of the banks (Fig. ). The developed algorithm, which uses, inter alia, an AutoHotkey  
265 script, will automatically launch the *srh-pre* and inputted SMS-exported files. The preprocessor stage will  
266 first check the possible errors and then output a directory file that contains the entire model input  
267 information, especially the topography. That file will be used to launch the processor *srh-2d* automatically.  
268 However, prior to that, the automation algorithm will make two principal modifications:

269 (1) The initial start time, time step and end time are among the simulation information stored on the  
270 directory file. The initial simulation end time will be automatically changed to the BISHOP time  
271 step  $\Delta t'$ . In addition, for the first run, the initial start time will be kept unchanged. However, starting  
272 from the second run, the start time will be the end time of the previous simulation, and the new  
273 end time will be  $\Delta t'$  plus the start time. The simulation will accordingly last  $\Delta t'$  of the flood event  
274 for each run. The algorithm will call up the BISHOP model (Mahdi 2004) to evaluate the bank  
275 stability at the end of each run. The program will launch SRH-2D several times ( $N_{b_{times}}$ ) and test  
276 the bank stability at the end of each run until the total number of times is equal to the ratio  
277 between the initial end time and the BISHOP time step  $\Delta t'$  ( $N_{b_{total}}$ ). It is worth noting that the  
278 chosen time step  $\Delta t'$  should preferably be a divisor of the initial end time if not the hydraulic time  
279 step.

280 (2) In addition to time information, the directory file records the name of the restart file, a file created  
281 by the SRH-2D model in a previous simulation using the same mesh and hydraulic conditions.  
282 The name of the file will be changed to the case name followed by *\_RST1*. During each SRH-2D  
283 simulation, the restart file is generated at each interval specified within the model control. Herein,  
284 this file will be generated only at the end of each run and will be used as the initial condition of the  
285 next simulation. This allows a continuation from the end of the previous simulation and thus takes  
286 into account the last hydraulic-sediment transport conditions.

287 Following these few changes in the directory file, the program will launch the SRH-2D model for the first  
288 run. The vertical model proceeds in its own time until it reaches the bank time step, when the BISHOP  
289 model is activated. The SRH-2D model outputs a results file that describes the time-dependent evolution  
290 of the cross-sections. The developed program will compare the node elevations of the cross-sections with  
291 the initial elevation. In the absence of erosion, the analysis is advanced for the next time step, as  
292 illustrated in the flowchart (Fig. ). If erosion occurs, at least around one riverbank, the new sections  
293 representing the bed at the end of the time step are tested for the stability of their banks. The new cross-  
294 sections will be divided into two riverbanks from the lowest bed elevation (Node 6 in Fig. ). Each bank will  
295 be subsequently coupled with its corresponding pre-established geotechnical properties files to define the  
296 input files for BISHOP. Hence, the stability of the riverbank will be assessed; it will be performed under  
297 drained conditions for the first potential bank failure and under undrained conditions afterwards. In fact,  
298 after the first failure, the stability analysis will be performed using the resistance of the shear stress of the  
299 undrained materials. This is due to the decrease in the interstitial pressure that allows the bank to resist  
300 geometric changes over a certain timespan (Mahdi and Merabtene 2010) and then accounts for the  
301 protection afforded by the failed materials.

302 In the absence of rupture ( $FS > 1$ ), the simulation is advanced for the next time step (Fig. ). Otherwise, the  
303 bank profile will be reshaped based on the REDISSED (Mahdi 2004) submodel; the corresponding  
304 geometric file will be updated to account for the new bank profile. Although the program will renew the  
305 channel bed and bank topography based on the updated geometry, prior to that, the program will make  
306 necessary transformations (translation and rotation) to adapt the new node coordinates to their initial  
307 global system on the SMS. In addition, the bed topography of all the nodes located inside the sliding cone  
308 area will be automatically interpolated to accommodate bank failure as illustrated in figure 9; the mesh will  
309 therefore be updated before moving to the next hydraulic time step.

310 Once the bed topography is updated, the program will set the restart file as an initial condition to continue  
311 from the last hydraulic-sediment transport conditions and ultimately make necessary changes in the start  
312 and end times, as explained before. The simulation will run as many times as necessary until the initial  
313 end time is achieved (see the application section below).

## 314 **Application: case study**

315 The approach adopted to verify the coupling procedure was applied over a long-reach scale; 7 kilometers  
316 of river length extending from the Première Chute Dam to Lake Témiscamingue along the Outaouais  
317 River at Notre-Dame-du-Nord, Quebec, was considered. The study reach is characterized by the  
318 presence of cohesive sediments along the river, and the height of the local banks typically vary between  
319 35 m high near the dam and 15 m high at the entrance of Lake Témiscamingue. It is an interesting field  
320 site since the water never overflows, even in the case of dam failure; therefore, bank failures are the only  
321 risk for the riverside population.

## 322 **Model setup**

323 A 2D mesh initial solution domain representing the initial channel topography of the study area was  
324 prepared in the SMS. The solution domain includes the positions of the selected cross-sections, where  
325 the geotechnical stability analysis will be performed, modeled as straight segments moving downstream  
326 from right to left, where the 2D mesh node coordinates define the bank face geometry. Herein, 52  
327 irregularly spaced cross-sections were selected (including inlet and outlet transects), as shown in Fig. .  
328 The cross-sections were carefully chosen to consider the hydraulic features of the channel, they relatively  
329 represent the field domain as they present the same soil characteristics and riverbank slopes around  
330 them from field observations.

331 A time series discharge with a peak of approximately 9780 m<sup>3</sup>/s, which corresponds to the dam failure  
332 scenario, was imposed upstream (Fig. ). A constant surface elevation of 179 m was enforced downstream  
333 that corresponds to the water elevation in the lake. To represent the bed behavior, a constant Manning's  
334 roughness coefficient ( $n$ ) of 0.040 ( $d_{50}$ =160 mm) was used for the entire reach; it was estimated based  
335 on field observations in 2002 (Thibault, 2002); no calibration was needed. The sediment transport  
336 computation was carried out by using the Yang formula (Yang 1973), which is compatible with the bed  
337 material of the reach, which was assumed to be made of the same material as the riverbanks. Note,  
338 however, that the selection of the sediment transport equation is not important for the analysis below.  
339 Table 1 lists the grain size composition of the bed and bank material segregated into seven size classes

340 supported by SRH-2D (Lai 2010). The volumetric compositions considering the seven classes listed in  
341 Table 1 are 80%, 7%, 7%, 4%, 1%, 0% and 0%.

342 The geotechnical input parameters were prepared for each bank profile separately (104 bank profiles).  
343 They consist of a single homogeneous cohesive layer with measured properties supplemented by field  
344 test results carried out on some collected samples: effective cohesion  $c' = 1.6$  KPa; undrained cohesion  
345  $c_u = 9$  KPa; unit weight  $\gamma' = 18.6$  KN/m<sup>3</sup>; and interior effective friction angle  $\phi' = 32^\circ$ . The pore pressure  
346 ratio, the ratio of the pore water pressure to the overburden pressure, was set to its maximum value  $r_u =$   
347 0.45 (Fredlund and Barbour 1986). In this regard, we emphasize that within BISHOP (Mahdi 2004; Mahdi  
348 and Merabtene 2010), it is also possible to define pore water pressures given the pressure field or the  
349 groundwater table. Since information was not available, we assumed the most unfavorable case and  
350 chose the maximum pore pressure ratio.

351 The coupling procedure between SRH-2D (Lai 2010) and BISHOP (Mahdi 2004) was applied for 9 hours  
352 of the event. The flow, sediment transport and bed evolution time step was set to 5 s, whereas the  
353 stability analysis was carried out each  $\Delta t' = 0.125$  h. The time scale to assess the geotechnical stability of  
354 the banks is usually much greater than the time scales of hydrodynamic and channel bed morphological  
355 evolution. A sensitivity analysis will be conducted later to explore the impact of the time scale on the  
356 results of the model. Given the above values, the simulation will run 72 times ( $N_{b_{total}} = 9 / (\Delta t') = 72$ ), and at  
357 the end of each run, the stability analysis will be assessed profile by profile. As stated earlier, to update  
358 the flow-wise 2D geometry, a cone-shaped failure block was considered. Since there are no available  
359 measured data regarding the extents of the failed area and because the mesh is relatively coarser, a  $60^\circ$   
360 opening cone angle was assumed in the case of bank failures. Finally, the REDISSED parameter  $\alpha$  was  
361 set to 5.5 as suggested by (Thibault C et al. 2002) to represent the form of the failed banks at the study  
362 site.

## 363 **Results**

364 Two different scenarios were simulated. The first scenario considered only vertical erosion modeling  
365 using the SRH-2D (Lai 2010) model, and the second scenario combined vertical and lateral erosion  
366 modeling using the coupling procedure. **Error! Reference source not found.** shows the initial and final

367 profiles for selected riverbanks considering both scenarios, Fig. 13 shows the bank retreat plan view and  
368 Fig.14 shows a 3D view of a redefined bank profile. The evolution of the factor of safety for the riverbanks  
369 during the simulation period is illustrated in **Error! Reference source not found.** Furthermore, the  
370 predicted net bank retreat distances for all the cross-sections are displayed in Fig. .

371 These results show that bank failures are mostly observed alongside the bend and in the upstream  
372 section above it, where banks are high and steep. The bank retreat process was particularly significant  
373 within the river bend, which reveals a bank retreat up to 6 m for cross-sections 13 to 16, particularly on  
374 the right bank section (Fig. ). This can most likely be attributed to the optimal combination of slope and  
375 flow, to similarities in bank geometry and to the relatively narrower cross-sections in that area. In fact,  
376 fluvial erosion seems to have contributed more to steepening the bank profiles upstream, making them  
377 susceptible to geotechnical failures. Downstream, bank failures were almost absent, flow velocity and  
378 shear stress were smaller, bank heights and slopes were lower, and the channel morphological changes  
379 were then exclusively dominated by fluvial erosion.

380 Moreover, the erosion of the channel bed is noticeably stronger when exhibiting the bank failure process,  
381 especially for the first cross-sections (7R, 9L, and 9R) (hereafter denoting L for the left bank and R for the  
382 right bank) and along the bend (10L,10R and 14R). The failed bank-deposited materials downslope seem  
383 to serve as temporary protection from the fluvial erosion but make the cross-sections narrower and the  
384 slopes steeper, which increase the speed of the flowing water and the channel bed erosion rate.  
385 Furthermore, this rate appears to be related to the timing of the mass failure. In fact, the channel bed  
386 zone of the transects where the banks were predicted to fail early have been eroded more (9L, 14R, 23R  
387 and 28L) compared to those that failed later (1R and 9R) where the simulated bed deepening is  
388 approximately the same when considering the fluvial erosion only. This may be justified because the bank  
389 predicted to fail earlier becomes much more stable over the rest of the simulation period, which makes  
390 the channel narrower for a long period. Indeed, after the first bank failure, we hypothesize that bank  
391 stability will be evaluated with undrained conditions, which enhance the geotechnical stability of the bank.  
392 In addition, as stated above, the protection afforded by the failed materials further increases their stability,  
393 as the failed materials have to be removed first by fluvial erosion. Together, these findings explain the



394 slightly higher channel bed erosion rate for banks predicted to fail earlier compared to those that failed  
395 later.

396 Furthermore, after the bank failure, we note that the bank geometry was reshaped, and the failed blocks  
397 were redistributed along the cross-section. The redistribution of the eroded materials is clearly visible for  
398 the banks that failed later (1R and 9R) since the fluvial erosion did not consume all the material deposits.  
399 However, the volume of the failed bank materials is seen to be reduced for banks that failed earlier (14R,  
400 23R). In addition, the slump blocks have been redistributed all around the neighboring transects  
401 considering the failure cone shape assumption established in the process of this study. Fig. shows the  
402 bank geometry profile of the cross-sections neighboring the failed bank at cross-section 10, where the  
403 bed elevations of the mesh nodes were displaced to account for the newly defined bank profile.

#### 404 **Sensitivity to the BISHOP time step**

405 Sensitivity analysis was completed to determine the impact of the geotechnical stability analysis time step  
406 on the bank failure prediction and retreating distances. Simulations with different time steps were run  
407 using 0.0625, 0.125, 0.25 and 0.5 h. The selected time steps are all divisors of the simulation total time (9  
408 hours) to ensure having the necessary runs to reach it. Hence, the simulation was run 144, 72, 36 and 18  
409 times for each time step. By doing so, we reasonably hypothesize that the closer the BISHOP (Mahdi  
410 2004) time step is to the SRH-2D (Lai 2010) time step, the more we are certain to capture all the potential  
411 riverbank failures.

412 Fig. shows the retreating bank distances for the right and left top bank lines for different geotechnical  
413 time steps. Table 2 lists only riverbanks that were predicted to fail for certain time steps but not for others.  
414 As expected, more banks were predicted to fail while decreasing the BISHOP (Mahdi 2004) time step. In  
415 fact, the right bank at cross-section 7 and the left bank at cross-section 28 were predicted to fail for both  
416 time steps 0.0625 and 0.125 h but not for the highest time steps. Three and even four bank failures were  
417 missed for time steps of 0.25 and 0.5 h; the flow conditions have perhaps changed, and the banks are no  
418 longer unstable. However, we note that the left bank at cross-section 9 was predicted to fail when  
419 considering time step 0.125 but not time step 0.0625. This can be attributed to the BISHOP (Mahdi 2004)

420 order of accuracy. Fig. shows that the factor of safety was very close to unity; to three decimal places,  
421 the bank was considered, though, stable.

422 Moreover, the timing of bank failure seems to be accurately predicted using small time steps (0.0625 and  
423 0.125). Fig. shows the evolution of the factor of safety at the left bank of cross-section 10 considering the  
424 four configurations. The failure occurs 2.375 hours from the start of the simulation when using time steps  
425 of 0.0625 and 0.125 h. However, the riverbank was predicted to fail later for the two other time steps  
426 (almost one hour later). This can most likely be justified by the subsequent failures along the directly  
427 neighboring transects of the channel bank. In fact, the left bank of transect 9 was predicted to fail 2 hours  
428 after the simulation begins when using 0.0625 and 0.125 time steps but not for the highest time steps.  
429 This probably impacted the 10L bank failure time when using 0.25- and 0.5 time steps, as the channel  
430 bank form in that area was different. Although the 10L bank profile was slightly the same for the four  
431 different time steps (not shown), the difference between the timings was insignificant compared to the  
432 total remaining time of the simulation.

433 Overall, despite the timing issues highlighted above, we notice that the predicted bank retreat area and  
434 the retreating bank distances were considerably close for the small time steps (Fig. ). The model was  
435 nevertheless capable of capturing the potential troubling spots without regard to the chosen time step. We  
436 recommend, however, using small time steps to improve predictions of the retreat location with respect to  
437 the computational cost of the simulation.

## 438 **Discussion**

439 Despite the overall success in predicting the bank retreat and redistributing the removed unstable failure  
440 blocks, some aspects of the study need more attention. First, the predicted bank retreat depends on the  
441 mesh size considered. With the current mesh, the bank zone is badly represented, an average of ten  
442 lateral nodes define the transects, which unsatisfactorily capture the bank face geometry and would yield  
443 to a scarce bank retreating prediction. Second, after bank failure, only a few neighboring cross-sections  
444 were reshaped to account for the newly defined bank profile, perhaps because of the cone interior angle  
445 and again the mesh density. Indeed, we used a relatively coarser mesh, and few elements were affected.  
446 The mesh was locally refined at cross-section 10 to take account of the newly reshaped bank profile as

447 illustrated in Fig. 20; further mesh refinement may allow defining the sliding area accurately but increases  
448 the study computational cost and may induce model divergence, as the mesh representing the failed  
449 banks might be distorted considerably. The cone interior angle considered could affect the extent of the  
450 sliding area, especially for a much-refined mesh. The angle of  $60^\circ$  was set as an assumption in the  
451 present study, a sensitivity analysis might be conducted to evaluate the influence of the angle but it is  
452 outside the scope of this research. Third, after bank failure, the REDISSED (Mahdi 2004) submodel  
453 reshapes the bank profile as described in detail earlier, although the submodel adds some supplementary  
454 points to correctly represent the geometry of the bank face toward ensuring mass conservation. However,  
455 the elevation of those additional points will be used to shift the mesh node elevations using a simple  
456 linear interpolation method, which may induce loss of precision. Higher-order interpolation functions could  
457 potentially yield better accuracy but were abandoned during the study since it would be reasonable and  
458 suitable to combine the functions with a much finer mesh. Fourth, the fluvial erosion rate before and after  
459 the bank failure was considered the same, which might be incorrect as the critical shear stress of the  
460 materials differs, but this was also an assumption that we have made in the present research, which  
461 seems to be acceptable since it does not affect the objectives of the study. Finally, the pore pressure ratio  
462 was considered constant for all the banks, which might influence the bank failure prediction since  
463 cohesive banks are more susceptible to failure during rapid-drawdown, high-flow events (Alonso and  
464 Pinyol 2016). The constant pore pressure ratio was again an assumption that we considered in the  
465 present study and might be a subarea for future improvement.

466 Streambank erosion modeling of the river reach extending from the Première Chute Dam to Lake  
467 Témiscamingue along the Outaouais River was very challenging. The reach longitudinal length was  
468 approximately 7 km, the banks are very tall and steep, and landslides along this river reach are the  
469 predominant existing risk. Simulation of the river reach evolution was conducted considering a dam break  
470 scenario that requires a frequent decrease in the hydraulic time step to ensure model convergence.  
471 Notwithstanding those difficulties, up to 100 m of bank retreat was predicted at several riverbanks (Fig. ),  
472 and almost 20 cross-sections were reshaped using the developed coupling procedure. Typical results  
473 demonstrating the effectiveness of the developed methodology were presented in the study. Importantly,  
474 the model allows the automatic prediction of bank retreat due to both fluvial erosion and geotechnical

475 failure in long-reach-scale modeling systems using a 2D mesh in a simple and easy-to-use manner.  
476 Without survey data, the model is valid primarily for the identification of potential trouble spots for streams  
477 without necessarily requiring various input parameters.

## 478 **Conclusion**

479 In this paper, a new platform coupling a 2D mobile-bed modeling software, SRH-2D, a rotational failure  
480 analysis model, BISHOP, and a bank failure sediment-redistribution submodel, REDISSED, was  
481 developed. The major contributions are the redistribution of the slump blocks produced by riverbank mass  
482 failures onto the 2D mesh while conserving the mass; automation of the data exchanges between the  
483 different models, which makes the simulation less tedious; and finally, the robustness and ease of use of  
484 the model, which makes it applicable to practical stream events.

485 The developed coupling procedure has been applied to simulate the channel morphology of the  
486 Outaouais River at Notre-Dame-Du Nord; considering the complexities of the study site and the shortage  
487 of geotechnical and survey data, all four established objectives were nonetheless attained. The coupling  
488 approach showed encouraging results; up to 100 m of bank retreat was predicted, and the bank faces of  
489 over 20 cross-sections were renewed. However, the study can be further enhanced. In this field  
490 application, it has been noted that redistribution of unstable blocks is done merely along the failed banks,  
491 yet the bed elevations of only a few nodes of the neighboring cross-sections were updated. The study can  
492 accordingly be improved by integrating a more accurate submodel capable of evaluating the extent of the  
493 slumped area based on the real topography and soil properties, which could be an interesting area of  
494 future research. Moreover, given the influence of pore pressure on the factor of safety (Casagli et al.  
495 1999), it would be beneficial to improve the BISHOP model by coupling it to a hydrogeological model  
496 giving the distribution of interstitial pressure in the soil instead of fixing a constant pore pressure ratio for  
497 all the riverbanks during the simulation period. Finally, nonfluvial processes such as seepage or rainfall  
498 events were not included in this study. Those processes could also impact the streambank erosion  
499 predictions; the fluvial process-based models alone are insufficient. Modeling those nonfluvial processes  
500 is another avenue for future research.

501        **Acknowledgment**

502        This research was supported in part by a National Science and Engineering Research Council (NSERC)  
503        Grant and *Hydro-Quebec*.

504        **Notation**

505        The following symbols are used in this paper:

506         $b_i$         Slice width

507         $c'$         Effective cohesion

508         $c'_i$         Effective cohesion of the slice

509         $c_u$         Undrained cohesion

510         $d$         Distance between two mesh nodes

511         $d_{50}$         Diameter at which 50% of a sample's mass is comprised of smaller particles

512         $FS$         Factor of Safety

513         $H$         The failure height

514         $i$         Slice

515         $L$         Left bank

516         $Nb_{times}$         Number of times to launch SRH-2D

517         $Nb_{total}$         The total number of times to launch SRH-2D

518         $R$         Right bank

519         $r_u$         Pore pressure ratio

520         $u_i$         Pore pressure ratio at the bottom of the slice

521	$W_i$	Slice Weight
522	$Z$	Mesh node elevation
523	$\alpha$	Coefficient greater than the unity, specified by the user based on field observation
524	$\alpha_i$	Angle between the vertical and the radius of the circular slip surface
525	$\phi'$	Interior effective friction angle
526	$\phi'_i$	Interior effective friction angle of the slice
527	$\gamma'$	Saturated unit weight
528	$\Delta t'$	Time step to test banks stability

## 529 **References**

- 530 Abad, J. D., and Garcia, M. H. (2006). "RVR Meander: A toolbox for re-meandering of channelized  
531 streams." *Computers & Geosciences*, 32(1), 92-101.
- 532 Alonso, E. E., and Pinyol, N. M. (2016). "Numerical analysis of rapid drawdown: Applications in real  
533 cases." *Water Science and Engineering*, 9(3), 175-182.
- 534 AQUAVEO (2019). "SMS 12.3 - The Complete Surface-water Solution.",  
535 <<http://www.aquaveo.com/software/sms-surface-water-modeling-system-introduction>>. (June 10,  
536 2019).
- 537 ASCE Task Committee on Hydraulics, B. M., and Modeling of River Width Adjustment (1998). "River  
538 width adjustment II: Modeling." *Journal of Hydraulic Engineering*, 124(9), 903-917.
- 539 Casagli, N., Rinaldi, M., Gargini, A., and Curini, A. (1999). "Pore water pressure and streambank stability:  
540 results from a monitoring site on the Sieve River, Italy." *Earth Surface Processes and Landforms:  
541 The Journal of the British Geomorphological Research Group*, 24(12), 1095-1114.
- 542 Darby, S. E., and Delbono, I. (2002). "A model of equilibrium bed topography for meander bends with  
543 erodible banks." *Earth Surface Processes and Landforms: The Journal of the British  
544 Geomorphological Research Group*, 27(10), 1057-1085.
- 545 Darby, S. E., Rinaldi, M., and Dapporto, S. (2007). "Coupled simulations of fluvial erosion and mass  
546 wasting for cohesive river banks." *Journal of Geophysical Research: Earth Surface*, 112(F3).
- 547 Fredlund, D. (1995). "User's guide SLOPE/W." *GEO-SLOPE International, Ltd., Calgary, Alb.*
- 548 Fredlund, D., and Barbour, S. (1986). "The prediction of pore pressure for slope stability analysis." *Proc.,  
549 Slope Stability Seminar, Univ. of Saskatchewan, Saskatoon, SK.*

- 550 Galland, J.-C., Goutal, N., and Hervouet, J.-M. (1991). "TELEMAC: A new numerical model for solving  
551 shallow water equations." *Advances in Water Resources*, 14(3), 138-148.
- 552 Highland, L., and Bobrowsky, P. T. (2008). *The landslide handbook: a guide to understanding landslides*,  
553 US Geological Survey Reston.
- 554 Lai, Y. (2008). "SRH-2D version 2: Theory and User's Manual, Sedimentation and River Hydraulics—Two-  
555 dimensional River Flow Modeling." *US Department of the Interior, Bureau of Reclamation,*  
556 *Technical Service Center, Denver, CO.*
- 557 Lai, Y. (2017). "Modeling Stream Bank Erosion: Practical Stream Results and Future Needs." *Water*,  
558 9(12), 950.
- 559 Lai, Y. G. (2010). "Two-dimensional depth-averaged flow modeling with an unstructured hybrid mesh."  
560 *Journal of Hydraulic Engineering*, 136(1), 12-23.
- 561 Lai, Y. G., Greimann, B. P., and Wu, K. (2010). "Soft bedrock erosion modeling with a two-dimensional  
562 depth-averaged model." *Journal of Hydraulic Engineering*, 137(8), 804-814.
- 563 Lai, Y. G., Smith, D. L., and Israel, J. (2016). "2D and 3D Flow Modeling of the Sacramento River  
564 Fremont Weir Section." *Proc., World Environmental and Water Resources Congress* 421-432.
- 565 Lai, Y. G., Thomas, R. E., Ozeren, Y., Simon, A., Greimann, B. P., and Wu, K. (2012). "Coupling a two-  
566 dimensional model with a deterministic bank stability model." *Proc., Proceedings of the ASCE*  
567 *World Environmental and Water Resources Congress, Albuquerque, NM, USA*, 1290-1300.
- 568 Lai, Y. G., Thomas, R. E., Ozeren, Y., Simon, A., Greimann, B. P., and Wu, K. (2015). "Modeling of  
569 multilayer cohesive bank erosion with a coupled bank stability and mobile-bed model."  
570 *Geomorphology*, 243, 116-129.
- 571 Langendoen, E. J. (2000). *Concepts: Conservational channel evolution and pollutant transport system*,  
572 USDA-ARS National Sedimentation Laboratory.
- 573 Langendoen, E. J., Mendoza, A., Abad, J. D., Tassi, P., Wang, D., Ata, R., El kadi Abderrezzak, K., and  
574 Hervouet, J.-M. (2016). "Improved numerical modeling of morphodynamics of rivers with steep  
575 banks." *Advances in water resources*, 93, 4-14.
- 576 Langendoen, E. J., and Simon, A. (2008). "Modeling the evolution of incised streams. II: Streambank  
577 erosion." *Journal of hydraulic engineering*, 134(7), 905-915.
- 578 Langendoen, E. J., Wells, R. R., Thomas, R. E., Simon, A., and Bingner, R. L. (2009). "Modeling the  
579 evolution of incised streams. iii: model application." *Journal of Hydraulic Engineering*, 135(6),  
580 476-486.
- 581 Lavoie, B., and Mahdi, T.-F. (2017). "Comparison of two-dimensional flood propagation models: SRH-2D  
582 and Hydro\_AS-2D." *Natural Hazards*, 86(3), 1207-1222.
- 583 Mahdi, T.-F. (2004). "Prévision par modélisation numérique de la zone de risque bordant un tronçon de  
584 rivière subissant une rupture de barrage [Prediction by numerical modeling of the risk zone  
585 bordering a section of river undergoing a dam break]." Ph.D. Thesis, Ecole Polytechnique de  
586 Montréal, Quebec, Canada.
- 587 Mahdi, T.-F., and Merabtene, T. (2010). "Automated numerical analysis tool for assessing potential bank  
588 failures during flooding." *Natural hazards*, 55(1), 3-14.
- 589 Mahdi, T., and Marche, C. (2003). "Prévision par modélisation numérique de la zone de risque bordant un  
590 tronçon de rivière subissant une crue exceptionnelle [Prediction by numerical modeling of the risk

591 zone bordering a section of river undergoing an exceptional flood]." *Canadian Journal of Civil*  
592 *Engineering*, 30(3), 568-579.

593 Moges, E. M. (2010). "Evaluation of sediment transport equations and parameter sensitivity analysis  
594 using the SRH-2D Model." Universität Stuttgart.

595 Motta, D., Abad, J. D., Langendoen, E. J., and Garcia, M. H. (2012). "A simplified 2D model for meander  
596 migration with physically-based bank evolution." *Geomorphology*, 163, 10-25.

597 Nagata, N., Hosoda, T., and Muramoto, Y. (2000). "Numerical analysis of river channel processes with  
598 bank erosion." *Journal of Hydraulic Engineering*, 126(4), 243-252.

599 Philipponat, G., and Hubert, B. (1979). "Fondation et ouvrage en terre." *Eyrolles*, 19-20.

600 Pizzuto, J. E. (1990). "Numerical simulation of gravel river widening." *Water Resources Research*, 26(9),  
601 1971-1980.

602 Rinaldi, M., Mengoni, B., Luppi, L., Darby, S. E., and Mosselman, E. (2008). "Numerical simulation of  
603 hydrodynamics and bank erosion in a river bend." *Water Resources Research*, 44(9).

604 Rousseau, Y. Y., Van de Wiel, M. J., and Biron, P. M. (2017). "Simulating bank erosion over an extended  
605 natural sinuous river reach using a universal slope stability algorithm coupled with a  
606 morphodynamic model." *Geomorphology*, 295, 690-704.

607 Simon, A., Curini, A., Darby, S. E., and Langendoen, E. J. (2000). "Bank and near-bank processes in an  
608 incised channel." *Geomorphology*, 35(3-4), 193-217.

609 Simon, A., Doyle, M., Kondolf, M., Shields Jr, F., Rhoads, B., and McPhillips, M. (2007). "Critical  
610 Evaluation of How the Rosgen Classification and Associated "Natural Channel Design" Methods  
611 Fail to Integrate and Quantify Fluvial Processes and Channel Response 1." *JAWRA Journal of*  
612 *the American Water Resources Association*, 43(5), 1117-1131.

613 Simon, A., Pollen-Bankhead, N., and Thomas, R. E. (2011). "Development and application of a  
614 deterministic bank stability and toe erosion model for stream restoration." *Stream restoration in*  
615 *dynamic fluvial systems*, 453-474.

616 Thibault C, Leroueil S, and J, L. (2002). "Évolution des berges de rivière en cas de rupture de barrage:  
617 cas du barrage Première-Chute." Université Laval, Québec.

618 Thorne, C. (1982). "Processes and mechanisms of river bank erosion." *Gravel-bed rivers*, 227-271.

619 Yang, C. T. (1973). "Incipient motion and sediment transport." *Journal of the hydraulics division*, 99(10),  
620 1679-1704.

621 Yang, C. T. (1976). "Minimum unit stream power and fluvial hydraulics." *Journal of the hydraulics division*,  
622 102(7), 919-934.

623 Yang, C. T., Trevino, M. A., and Simoes, F. J. (1998). *User's Manual for GSTARS 2.0 (Generalized*  
624 *Stream Tube Model for Alluvial River Simulation Version 2.0)*, US Department of Interior, Bureau  
625 of Reclamation.

626

627



628 **Figures Captions**

629 **Fig. 1.** Equilibrium of a soil layer (simplified Bishop method) (Mahdi 2004)).

630 **Fig. 2.** Initial geometry and circular failure (Scale-adjusted to display the details) ((Mahdi 2004)).

631 **Fig. 3.** Redistribution of the slump blocks following a circular failure (Scale-adjusted to display the details)  
632 ((Mahdi 2004)).

633 **Fig. 4.** Top view of the extents of the failed area defined within a cone-shaped form. The elevation of  
634 mesh nodes located in that area will be updated to account for the newly defined bank profile.

635 **Fig. 5.** The cross-sections before generating the mesh on the SMS.

636 **Fig. 6.** The cross-sections after generating the mesh on the SMS.

637 **Fig. 7.** The initial cross-section bed profile and the associated soil layers.

638 **Fig. 8.** The coupling procedure methodology.

639 **Fig. 9.** Sliding cone area and affected mesh nodes a) Plan view b) 3D view.

640 **Fig. 10.** The initial bathymetry for the Outaouais River at Notre-Dame-du-Nord, Quebec.

641 **Fig. 11.** The flood hydrograph at the upstream.

642 **Fig. 12.** The initial and final bank profiles for selected right and left riverbanks, and evolution of the factor  
643 of safety during the simulation period

644 **Fig. 13.** The predicted bankline changes after dam break occurrence (Red line) (retreats are 10 times  
645 exaggerated).

646 **Fig. 14.** The 3D view of a redefined bank profile.

647 **Fig. 2.** The predicted net bank retreat distances for all the predefined cross-sections.

648 **Fig. 3.** The left and right bank profiles for cross-sections upstream and downstream cross-section 10.

649 **Fig. 17.** The net bank retreat sensitivity to the BISHOP time step for the right and the left riverbanks.

650 **Fig. 18.** The evolution of the factor of safety of the right bank at cross-section 9.

651 **Fig. 19.** The evolution of the factor of safety of the right bank at cross-section 10 considering four different  
652 geotechnical time steps.

653 **Fig. 20.** Sliding cone area and affected mesh nodes before and after refining the mesh for cross section  
654 10.

655

656 **Tables Captions**

657 **Table 1.** Size ranges of seven sediment size classes used for the channel bed modeling.

658 **Table 2.** Riverbanks predicted to fail for different geotechnical time steps.

659

660

661

662 **Table 3.** Size ranges of seven sediment size classes used for the channel bed modeling

Sediment Size Class	Size Range (mm)
1	0.0025 to 0.0625
2	0.0625 to 0.125
3	0.125 to 0.25
4	0.25 to 0.5
5	0.5 to 1
6	1 to 2
7	>2

663

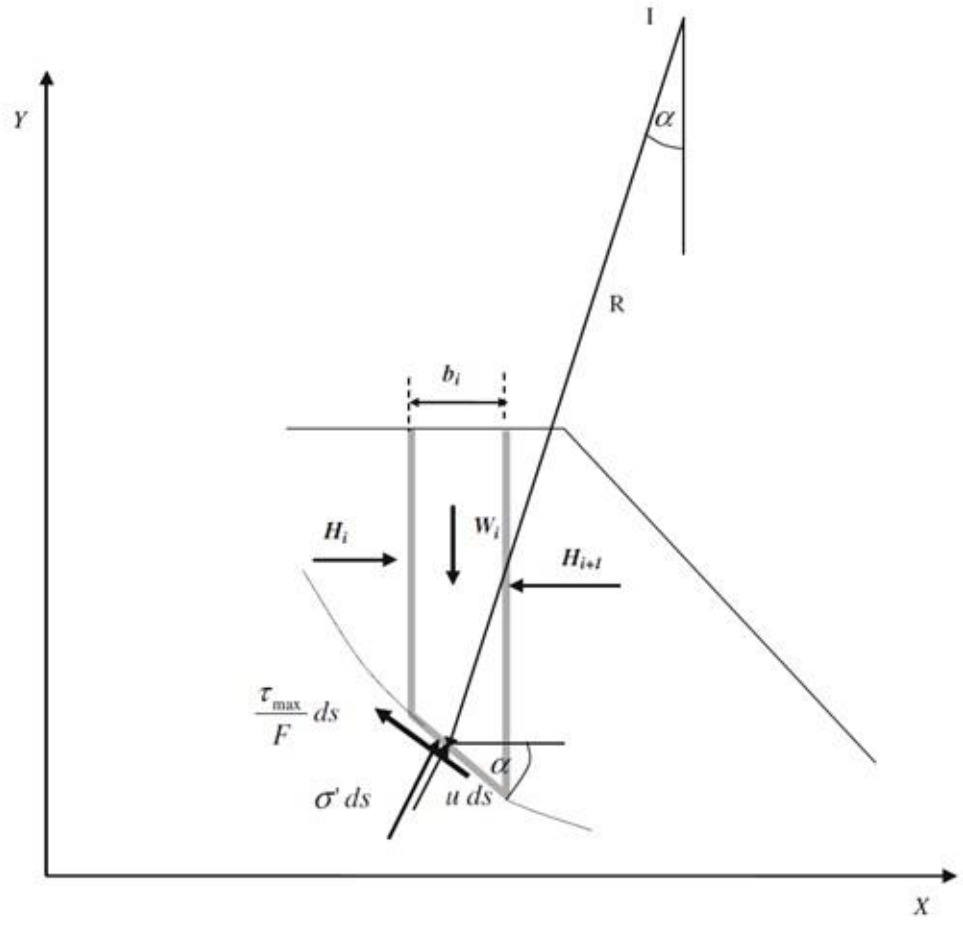
664

665 Table 2. Riverbanks predicted to fail for different geotechnical time steps. F: Failed banks; U: Unfailed banks.

BISHOP's time step(h)	Cross-sections																			
	1	6	7	9	10	11	12	13	14	15	16	21	23	24	25	26	27	28	29	
0.0625	F	F	F	U	F	F	F	F	F	F	F	F	F	F	F	F	F	F	F	
0.125	F	F	F	F	F	F	F	F	F	F	F	F	F	F	F	F	F	F	F	
0.25	F	F	U	U	F	F	F	F	F	F	F	F	F	F	F	F	F	F	U	F
0.5	U	U	U	U	F	F	F	F	F	F	F	F	F	F	F	F	F	F	U	F

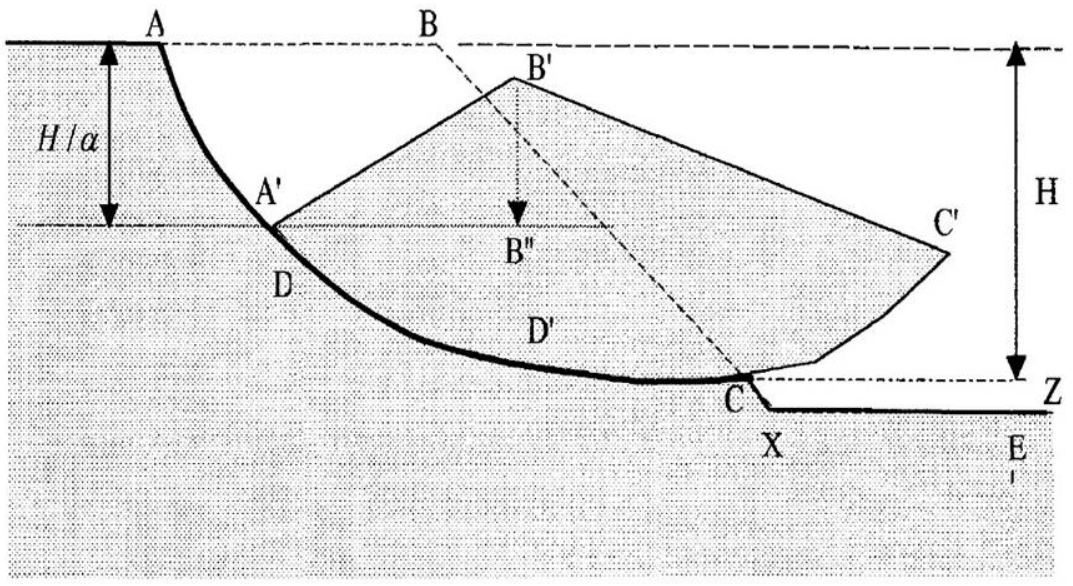
666

667



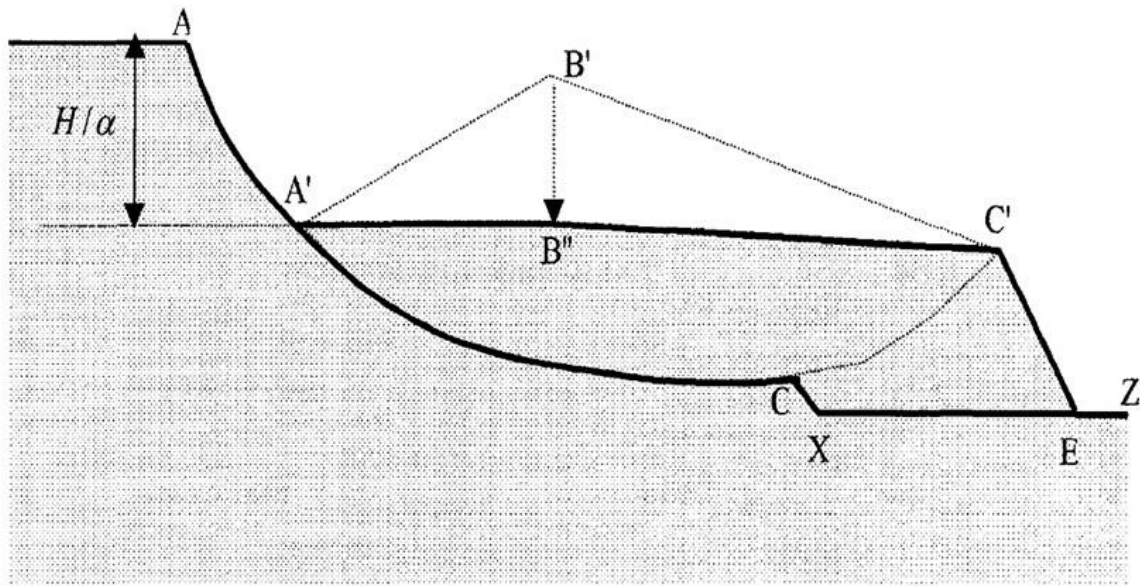
668

669 **Fig. 4.** Equilibrium of a soil layer (simplified Bishop method) (Mahdi 2004).

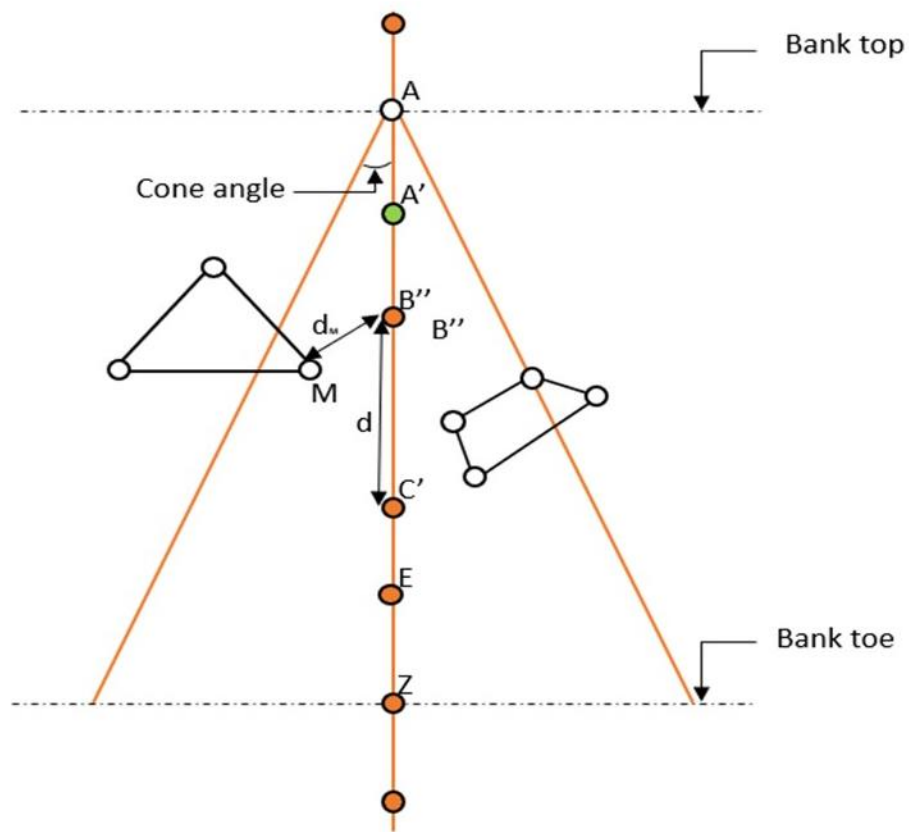


670

671 **Fig. 2.** Initial geometry and circular failure (Scale-adjusted to display the details) ((Mahdi 2004)).

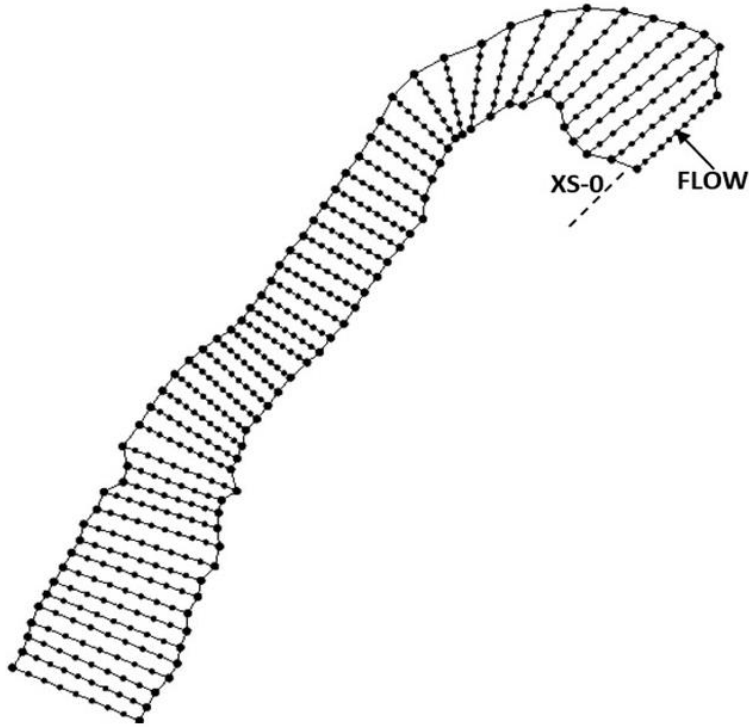


672  
 673 **Fig. 3.** Redistribution of the slump blocks following a circular failure (Scale-adjusted to display the details)  
 674 ((Mahdi 2004)).



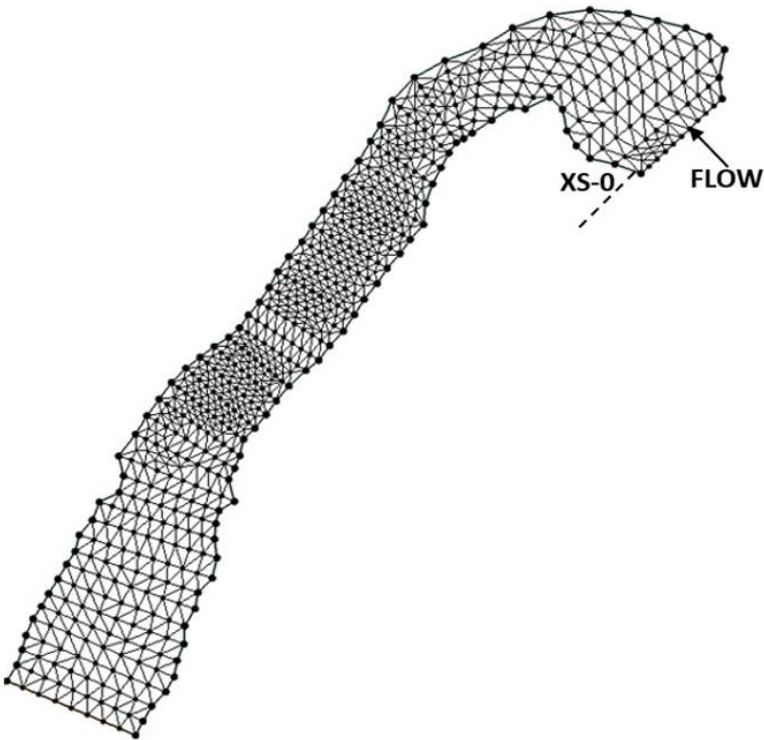
675  
 676 **Fig. 4.** Top view of the extents of the failed area defined within a cone-shaped form. The elevation of  
 677 mesh nodes located in that area will be updated to account for the newly defined bank profile.

678



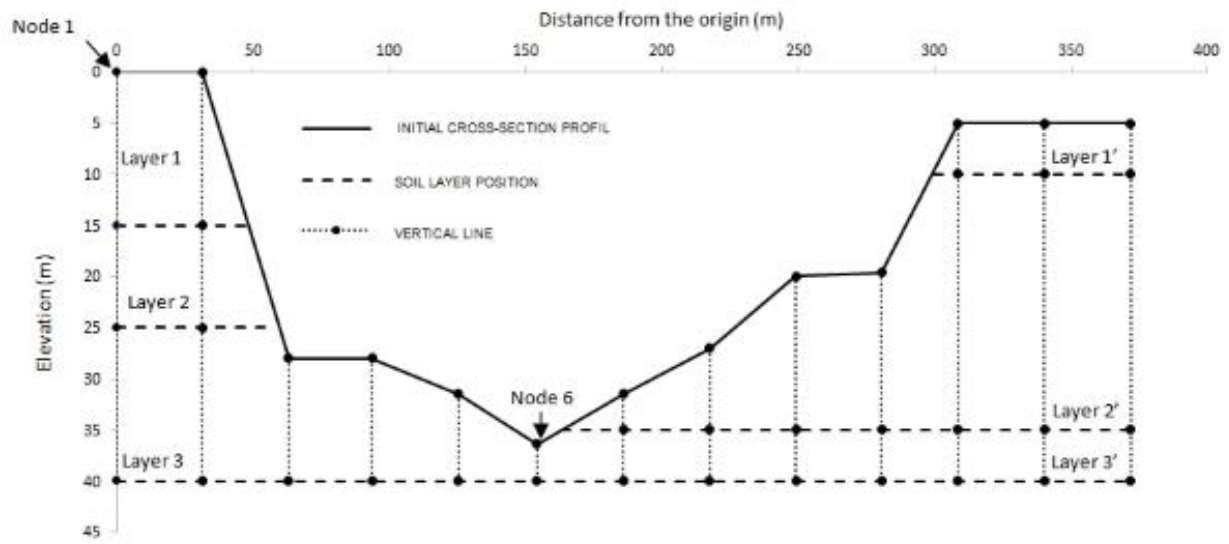
679

680 **Fig. 5.** The cross-sections before generating the mesh on the SMS.



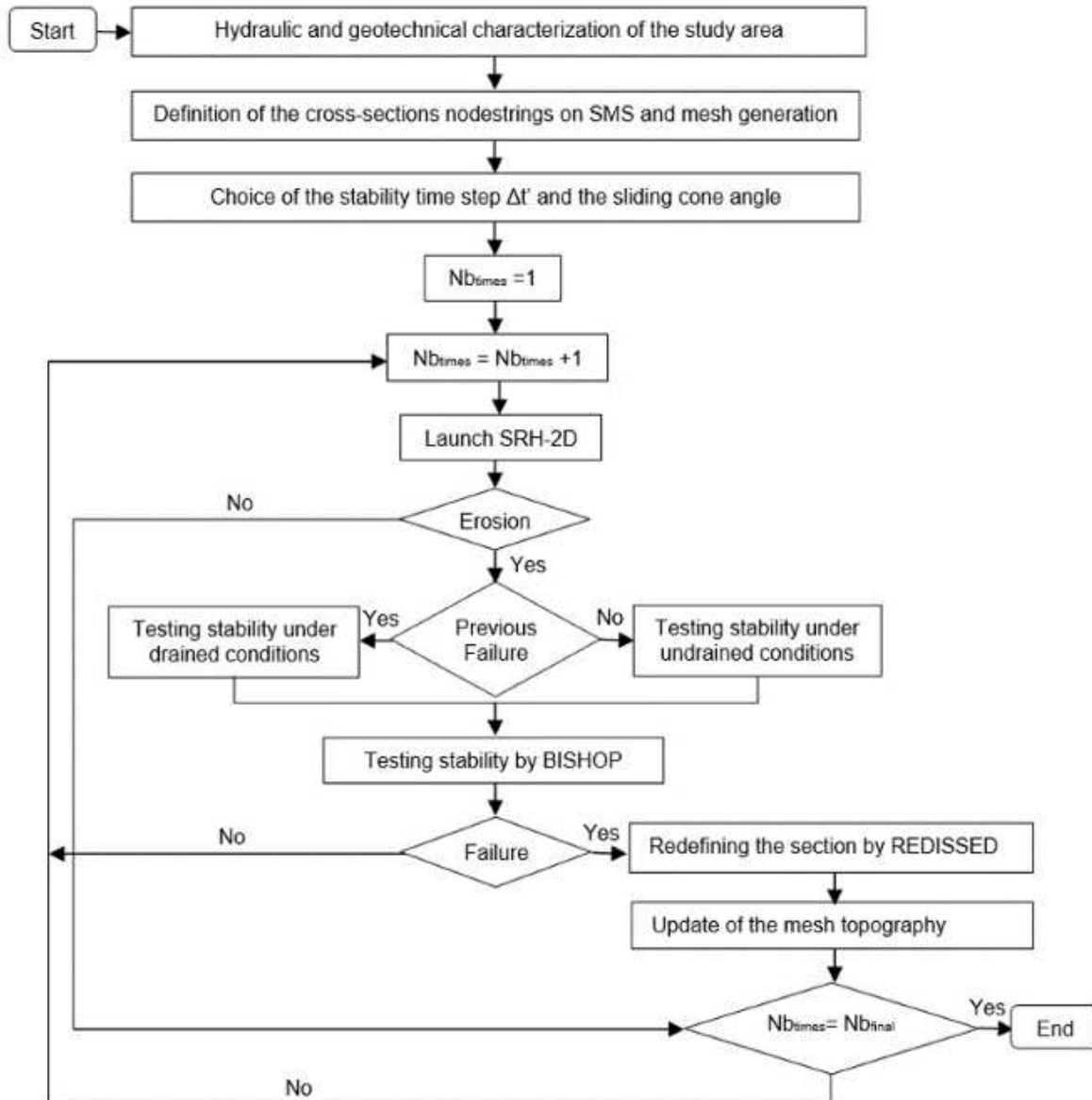
681

682 **Fig. 6.** The cross-sections after generating the mesh on the SMS.



683

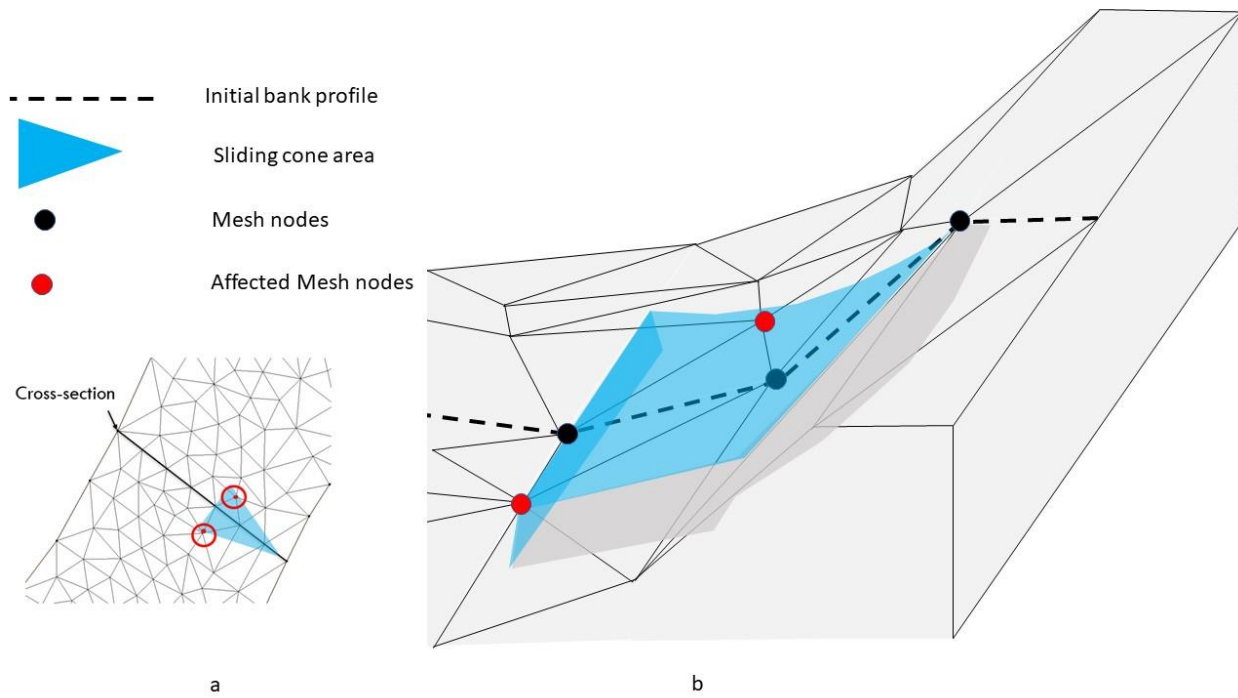
684 **Fig. 7.** The initial cross-section bed profile and the associated soil layers.



685

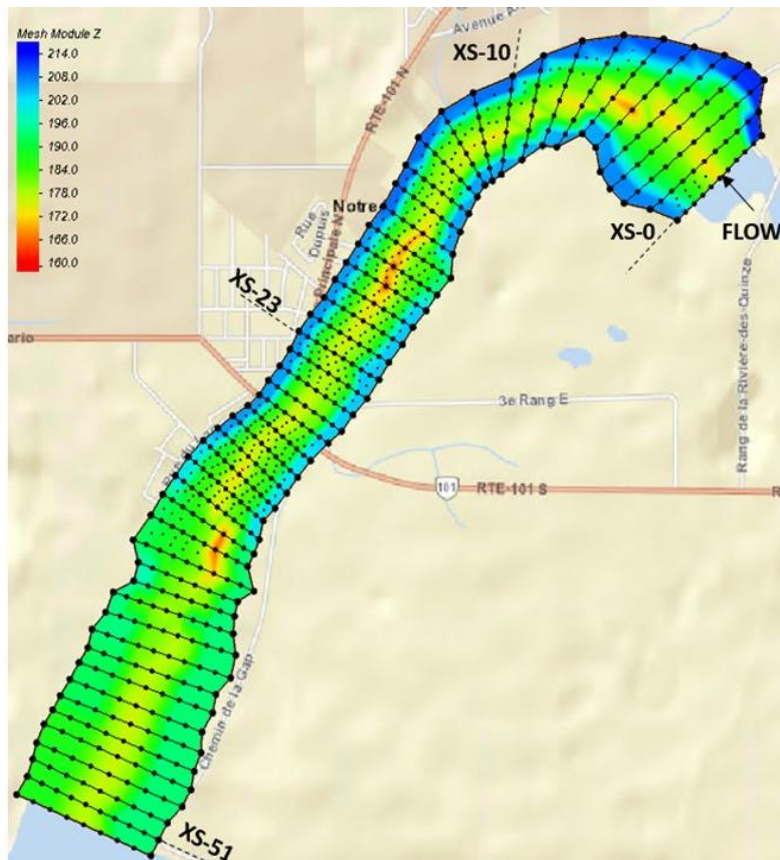
686 **Fig. 8.** The coupling procedure methodology.





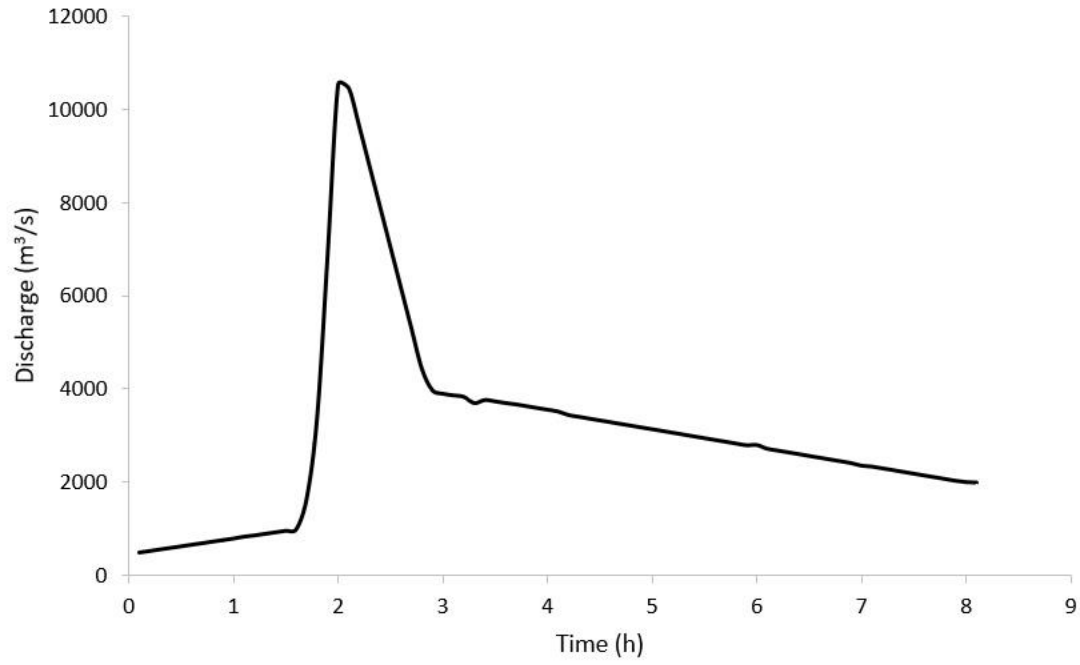
687

688 **Fig. 9.** Sliding cone area and affected mesh nodes a) Plan view b) 3D view.



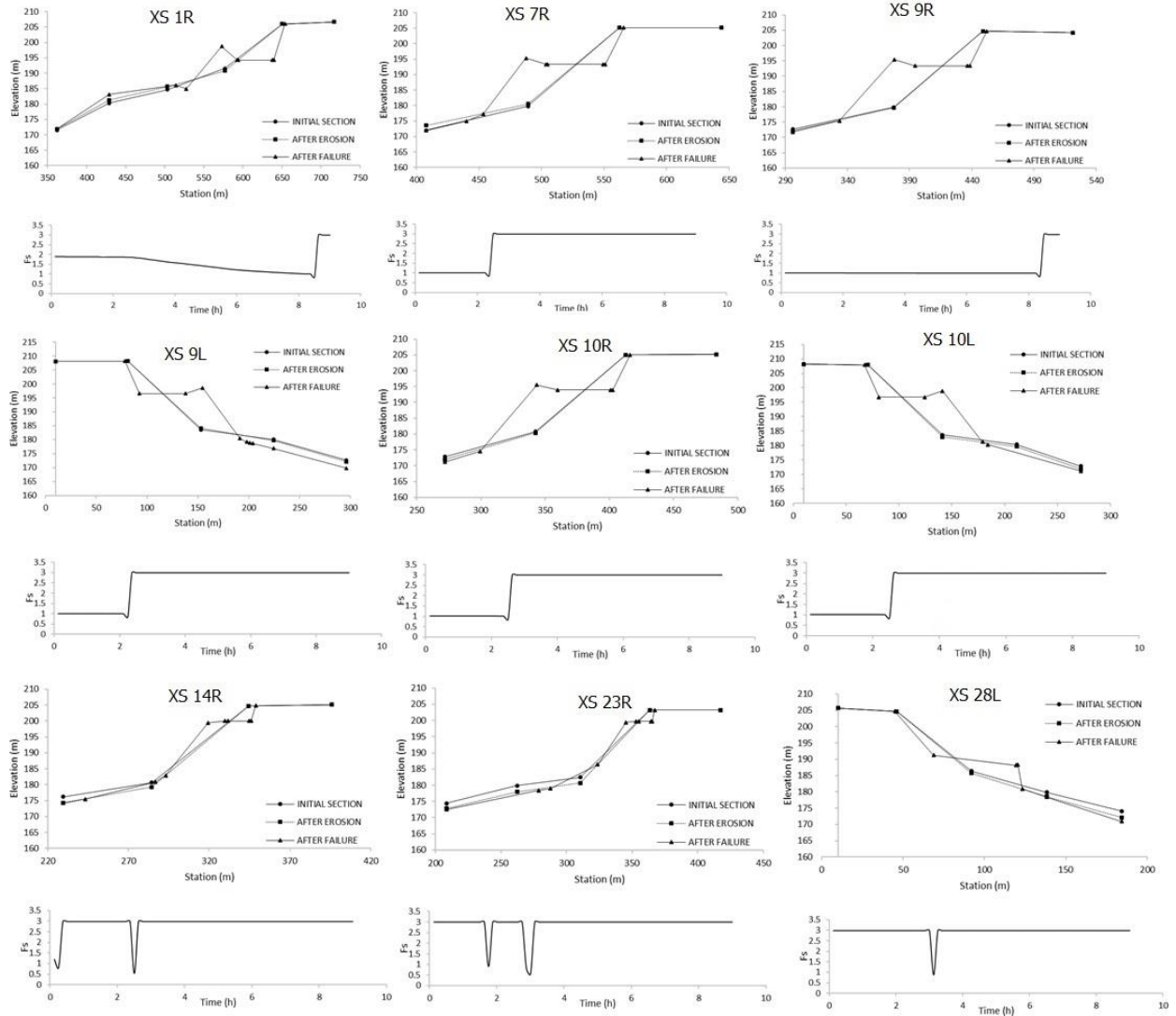
689

690 **Fig. 10.** The initial bathymetry for the Outaouais River at Notre-Dame-du-Nord, Quebec.



691

692 **Fig. 11.** The flood hydrograph at the upstream.

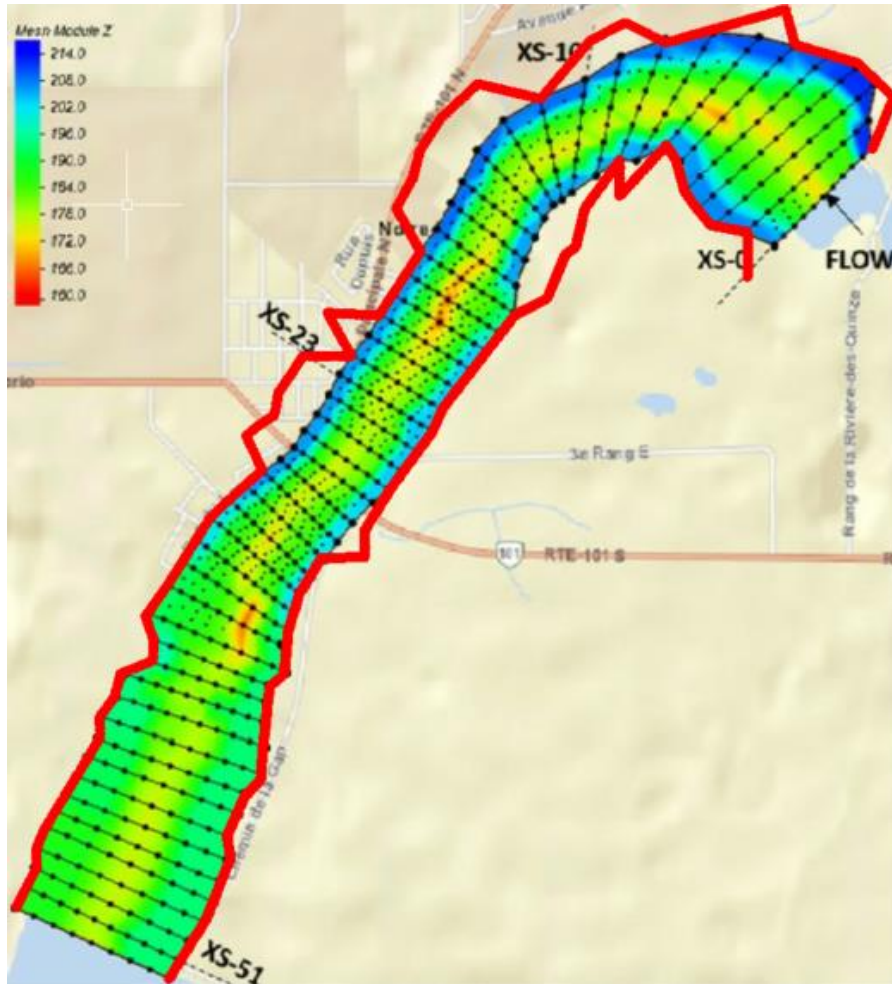


693

694

695

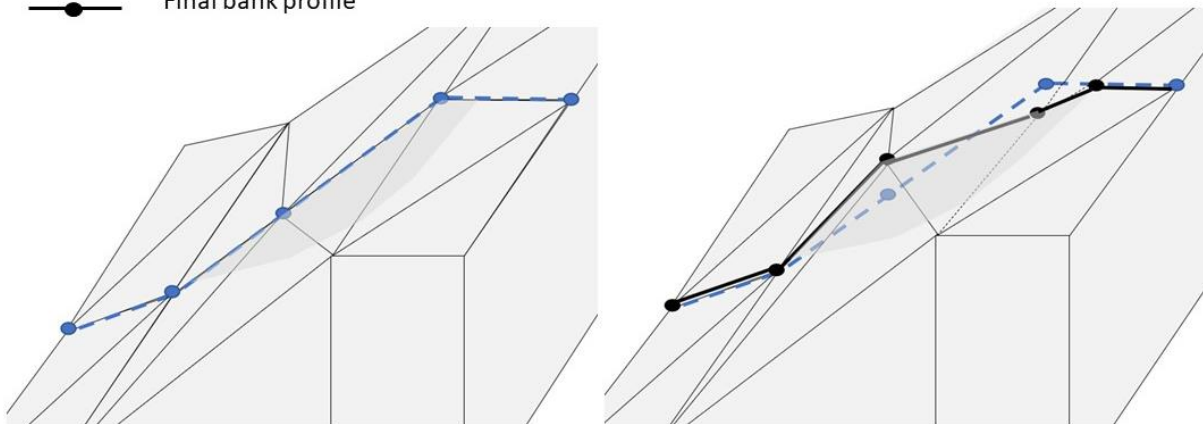
**Fig. 12.** The initial and final bank profiles for selected right and left riverbanks, and evolution of the factor of safety during the simulation period



696

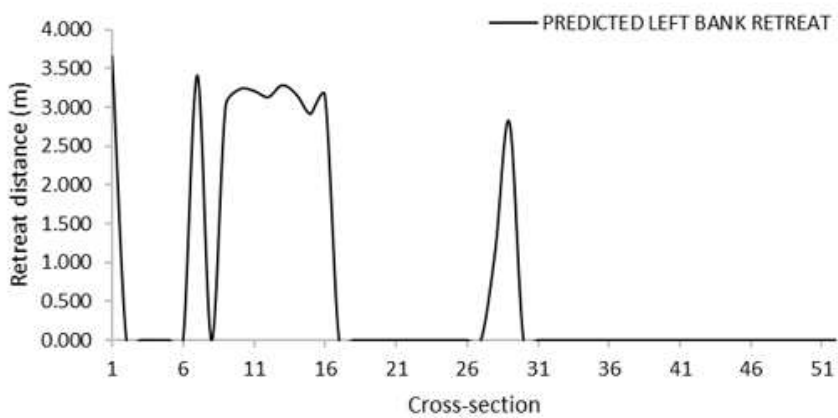
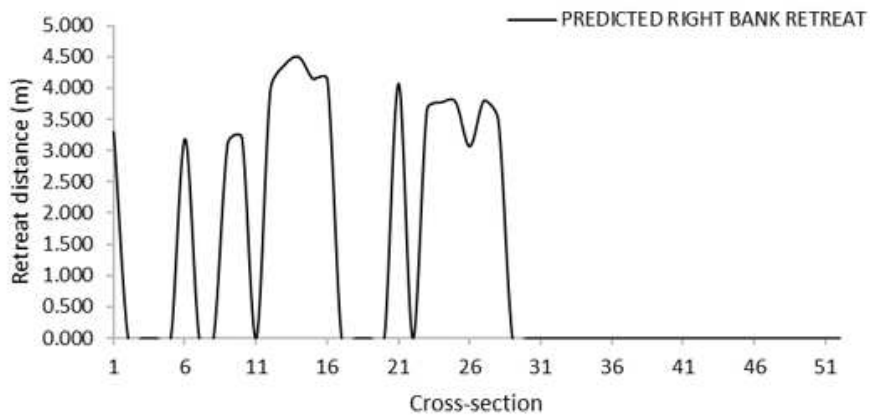
697 **Fig. 13.** The predicted bankline changes after dam break occurrence (Red line) (retreats are 10 times  
698 exaggerated).

- Initial bank profile
- Final bank profile



699

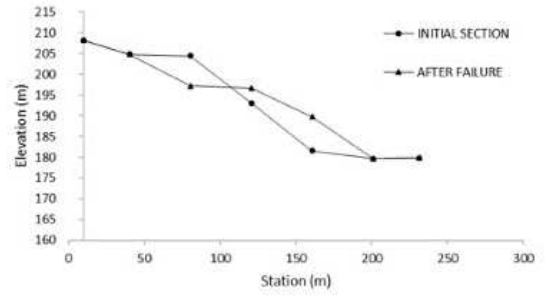
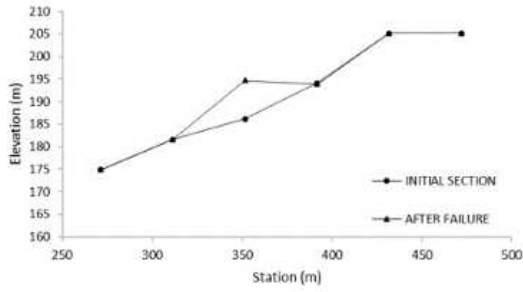
700 **Fig. 14.** The 3D view of a redefined bank profile.



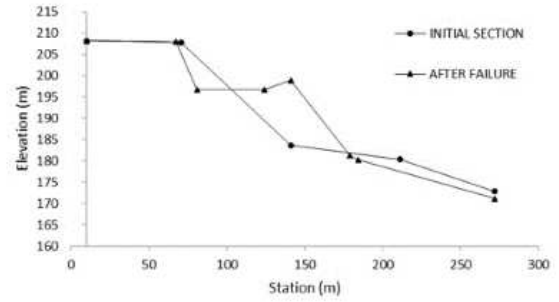
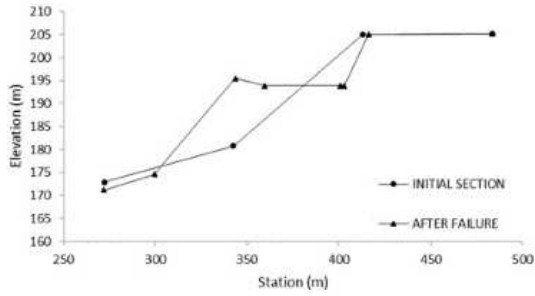
701

702 **Fig. 5.** The predicted net bank retreat distances for all the predefined cross-sections.

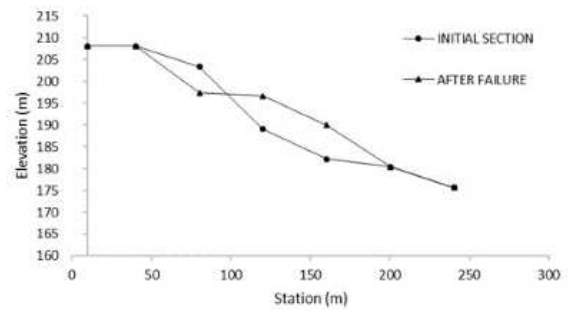
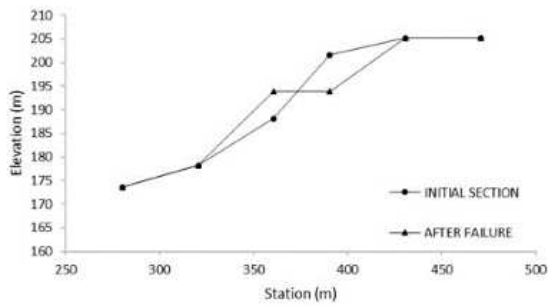
Upstream cross-section 10



Cross-section 10

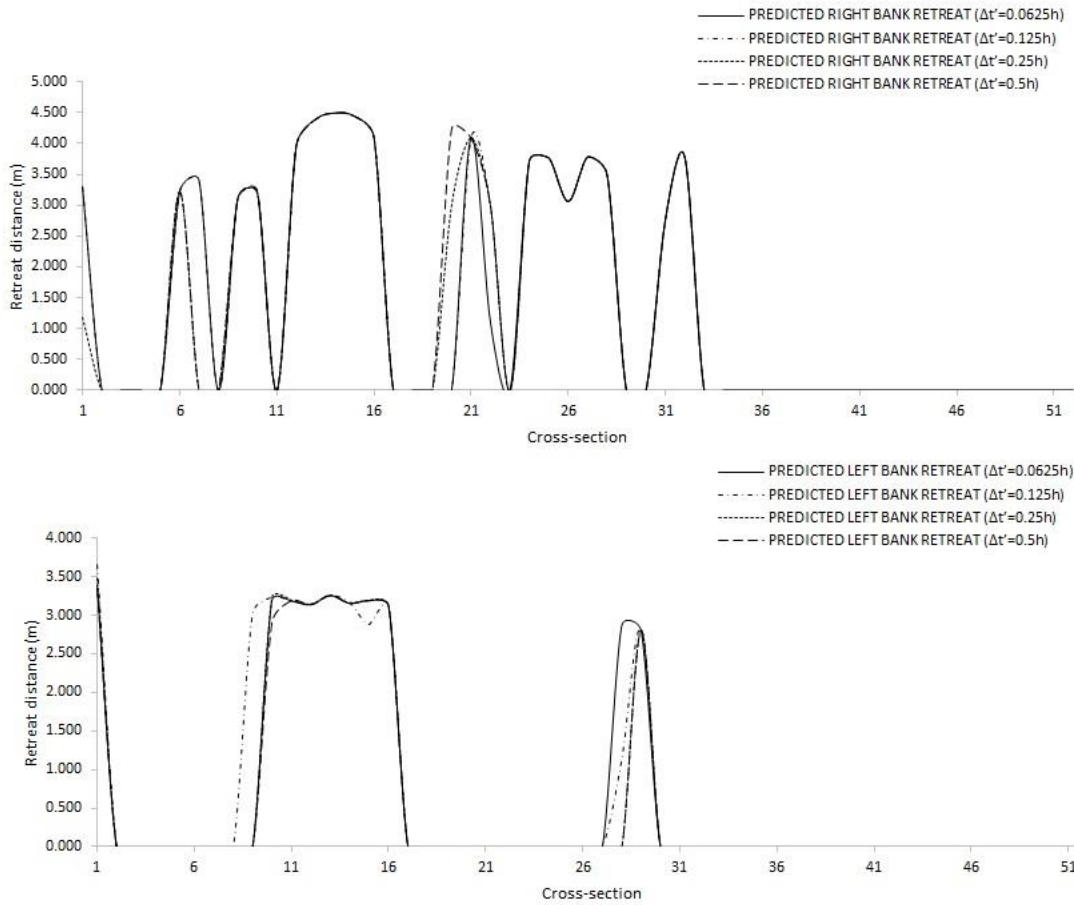


Downstream cross-section 10



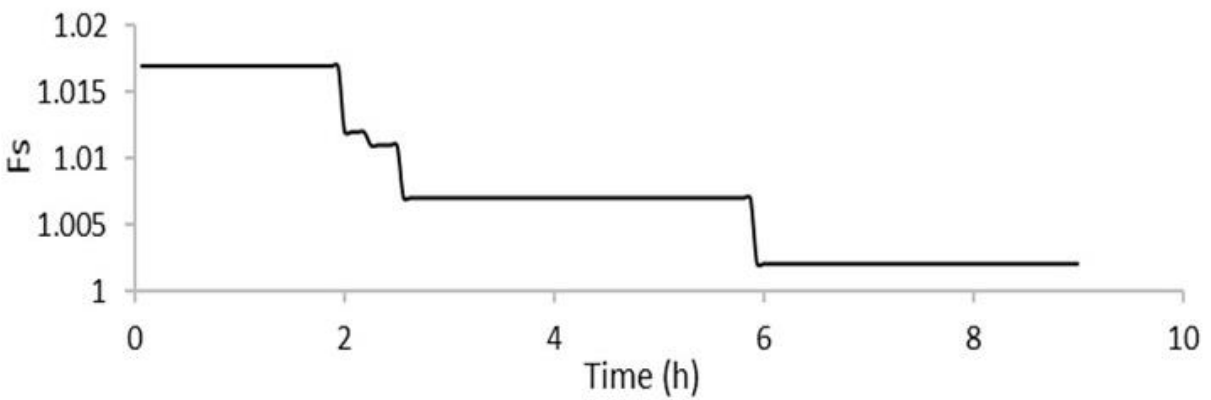
703

704 **Fig. 6.** The left and right bank profiles for cross-sections upstream and downstream cross-section 10.



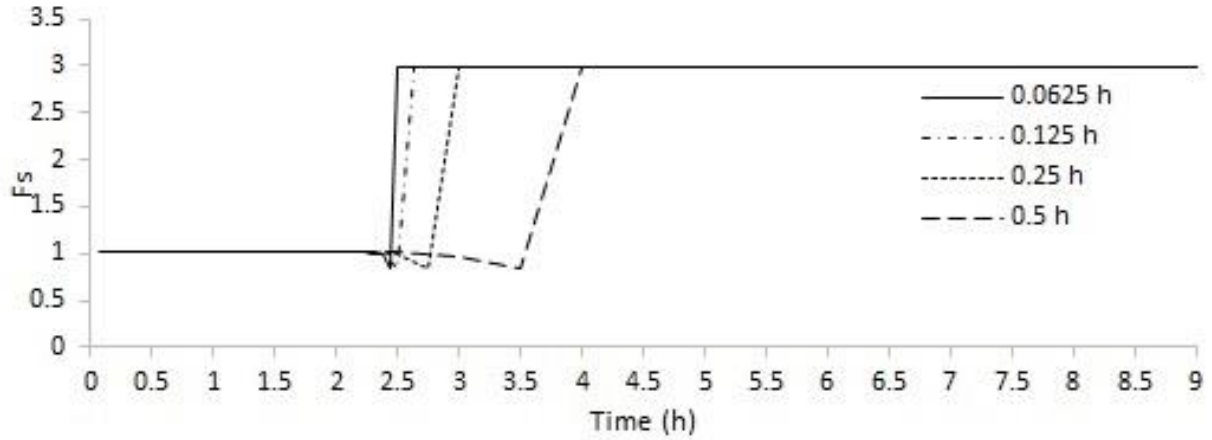
705

706 **Fig. 17.** The net bank retreat sensitivity to the BISHOP time step for the right and the left riverbanks.



707

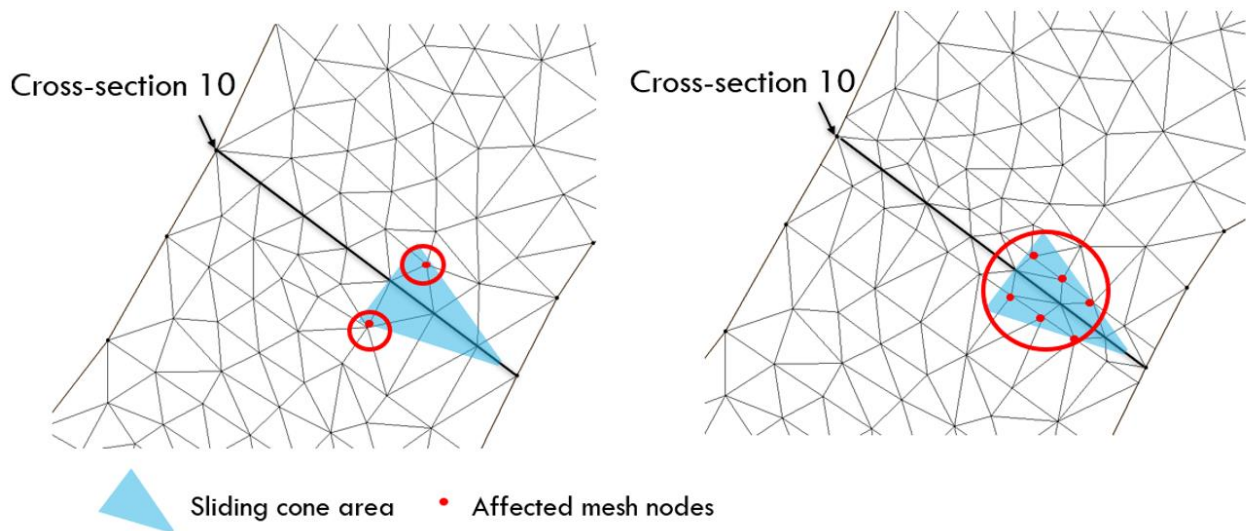
708 **Fig. 18.** The evolution of the factor of safety of the right bank at cross-section 9.



709

710 **Fig. 19.** The evolution of the factor of safety of the right bank at cross-section 10 considering four different  
 711 geotechnical time steps.

712



713

714 **Fig. 20.** Sliding cone area and affected mesh nodes before and after refining the mesh for cross section  
 715 10.

716